Phenotypic Analysis Combined with Tandem Mass Tags (TMT) Labeling Reveals the Heterogeneity of Strawberry Stolon Buds

Ling Guan (guanling@jaas.ac.cn)
Institute of Pomology, Jiangsu Academy of Agricultural Sciences

Research article

Keywords: Strawberry, Stolon buds, Phenotypic observation, Differentially expressed proteins, Tandem mass tags

Posted Date: June 27th, 2019

DOI: https://doi.org/10.21203/rs.2.10717/v1

Version of Record: A version of this preprint was published on November 19th, 2019. See the published version at https://doi.org/10.1186/s12870-019-2096-0.

Abstract

Background: Ramet propagation in strawberry (Fragaria × ananassa) is the most effective way in production. However, the lack of systematically phenotypic observations and high-throughput methods limits our ability to analyze the key factors regulating the heterogeneity in strawberry stolon buds. Results: From observation, we found that the axillary bud located in the first node quickly stepped into dormancy (DSB), after several bract and leaf buds were differentiated. The stolon apical meristem (SAM) degenerated as the new ramet leaf buds (RLB) and the new active axillary stolon buds (ASB) differentiated continually, after the differentiation of the first leaf. Using tandem mass tags (TMT) labeling method, totally 7,271 strawberry proteins were identified, and were used for further bioinformatics analysis in differentially expressed proteins (DEPs) between the groups of ASB and DSB, RLB and DSB, and RLB and ASB. Between ASB and DSB, the spliceosome DEPs, such as Ser/Arg-rich (SR) and heterogeneous nuclear ribonucleoprotein particle (hnRNP), showed the highest enrichment and high PPI connectivity. This indicated that the differences in DEPs (e.g., SF-3A subunit 2 isoform X1, hnRBP C1827.05c, and PK, cytosolic isozyme) at the transcriptional level may be causing the differences between the physiological statuses of ASB and DSB. As expected, the photosynthetic pre-form RLB mainly differentiated from ASB and DSB judging by the DEP enrichment of photosynthesis. However, there are still other specialized features of DEPs between RLB and DSB and between ASB and DSB. The DEPs relative to DNA duplication [e.g., minichromosome maintenance protein (MCM 2, 3, 4, 7)], provide a strong hint of functional gene duplication leading the bud heterogeneity between RLB and DSB. In addition, the top fold change in DEP LSH 10-like protein might be involved in the degeneration of SAM into RLBs. As for RLB/ASB, the phenylpropanoid biosynthesis pathway probably regulates the ramet axillary bud specialization, and further promotes the differentiation of xylem when ASB develops into a new stolon [e.g., cinnamyl alcohol dehydrogenase 1 (CAD1) and phenylalanine ammonia-lyase 1 (PAL1)]. Conclusions: The definite dormancy phase of DSB, and the biological pathways and gene networks that might be responsible for stolon buds heterogeneity were also revealed.

Background

Strawberry is a sequenced member of Rosaceae, characterized by perennial evergreen, diminutive herbaceous plants amenable to genetic transformation. It has a relatively small genome (*Fragaria vesca* ~240 Mb, *F.* × *ananassa* ~700 Mb) and shares substantial sequence identity with the other economically important rosaceous plants[1, 2]. It is widely used as a preference model plant by horticultural researchers. The cultivated strawberry, *F.* × *ananassa*, originated ~250 years ago, is among the youngest crop species, characterized by a highly nutritive large fruit, ease of vegetative propagation, and high economic value and is wildly and commercially produced by 76 countries in the world[3, 4]. Because of the high heterozygosity of strawberry cultivars, it will be caused high variability and genetic segregation in the progeny seedlings. Thus, the sexual reproduction by seeds is not suitable for strawberry production. Instead, stolon (elongated stems) vegetative propagation was usually and efficiently used to produce clonal ramets from an aerial stolon (runner). However, the bud in the first node of cultivated strawberry (*F.* × *ananassa*) stolon usually remains in dormancy, and only the buds of the second node have the ability to form ramets[4]. Thus, new insights into the mechanisms underlying the stolon bud decision to produce either dormant or active buds for forming plantlets are crucial for improving strawberry productivity.

Morphologically, a strawberry stolon is a special lateral branch of crown, which is originated from the mother plant's axillary meristems with its subtending nodal ramet structure[5, 6]. Anatomically, a strawberry stolon consists of a large proportion of thick cortex and a relatively small proportion of phloem, xylem, and pith for transporting water, ions, and photoassimilates between the mother plant and ramets[7, 8]. The process of forming ramets in the second node of strawberry stolon can be summarized as follows: the second node degenerates into the first leaf of a future ramet and is wrapped up by its bracts. The adventitious roots are formed from the bases of the second nodes. Upon the completion of the rooting process, the lateral bud on the second node begins to elongate as the next new stolon. This newly formed stolon is not a continuous part of the mother plant, but is the lateral buds located on the first plantlet's axil. After that, the second or third ramets can be sequentially formed under favorable environmental conditions[4].

Former studies on strawberry stolon were mostly focused on the mechanism of its formation or on the dictates of the flowering-runnering decision. According to a recent study, the DELLA protein seems to be an important factor controlling runner formation during asexual reproduction in strawberry[9]. The gibberellic acid (GA) biosynthesis in the axillary meristem is essential for inducing stolon differentiation. The possibility of the *FveGA20ox4* gene regulating the runnering-flowering decision in strawberry has been revealed[6]. The studies on the differences between the first and second nodes of strawberry stolon have always focused on the internode differences instead of the differences between buds. For example, Fang et al. (2011) used two-dimensional gel electrophoresis for comparing the proteomic profiles of the strawberry stolon internodes I-1 and I-2[10]. They found that the ubiquitin-proteasome and sugar-hormone pathways might be important during adventitious root formation at the second node of new clonal plants. By quantifying the movement of resources and their allocation between mother plants and daughter ramets along *Fragaria* stolons with respect to hierarchy, the results showed that the stolon anatomy develops rapidly at the apical end, facilitating hierarchical ramet development, which is evident as a basipetal increase in hydraulic conductivities. The rapid development of transport tissue functionality enables young unrooted ramets to acquire water, as well as mineral ions disproportionally with respect to older ramets, in order to supply an expanding leaf area [8]. However, the mechanism by which the first node buds of cultivated strawberry usually remain in dormancy is not clear, and even when this dormancy is released under favorable environment, the first node buds have no ability to form ramets, but how they develop into new stolon branches is still unclear. In addition, the regulation of the mechanism underlying the dormancy of a stolon branch bud in the first node, but activity in the newly formed ramet located in the second node, is not clearly understood.

Thus, we first elucidated the developmental characterizations of the first and second node buds at different developmental stages, by using anatomical observation. Subsequently, we illustrated the definite dormancy phase of the first node bud, and the detailed developmental processes of the ramet formation and ramet axillary bud elongation in the second node of strawberry stolon, using stereomicroscopy and scanning electron microscopy. Considering the proteomics utilization, especially the tremendous advantages in method of TMT in digging the DEPs among multiple groups of plant materials[11-15]. In the last part, we mainly laid the foundation for understanding the mechanisms of strawberry stolon phenotype and bud development at the protein level. By using phenotypic observation combined with proteomic networks with different types of strawberry stolon buds, the definite dormancy phase of DSB was identified, and the biological pathways and gene networks that might be responsible for heterogeneity among different stolon buds in strawberry were also revealed.

Results

Stolon anatomy

The anatomical observation showed that the first node of the stolon (10 cm length) in cultivated strawberry (*F.* × *ananassa* Duch.) was extremely small and easily ignorable. When the bract of the first node was peeled off, a very tiny bud (Fig. 1*A*) was observed. On the contrary, for the observation of the second node, two different types of buds were observed underneath the bract—one was a plump bud (Fig. 1*B*), and the other was a leaf cluster mixed with several developing leaf buds (Fig. 1*C*). The slice observation showed that the buds in the first node stopped growing and stepped into dormancy at an early stage (Fig. 2*A*). The dormancy of the bud located at the first node could be released only under favorable environmental conditions, and it continues to develop into a new stolon branch (Fig. 2*B*). The leaf buds, located inside of the bract of the second node, have a distinct trifoliolate structure (Fig. 2*C*), and the vascular bundles of the newly formed stolon, which is laterally located on the leaf buds, are connected inward with the primary stolon (Fig. 2*D*). The structure of the strawberry stolon was observed by cross-sectional anatomy. The tissues from outside to inside of the stolon included epidermal hair and epidermis, thick cortex, cambium, phloem, xylem, and the pith, which are composed of a large number of parenchymatous cells (Fig. 2*E*). These two types of lateral buds on the first and second nodes of stolon were inwardly connected with the primary stolon in a same pattern (Figs. 2*F-G*). At the base of the second node, which is connected to the terminal strawberry stolon buds, there are numerous adventitious root primordia (Figs. 2*H-I*). Each adventitious root primordium originated from the cambium tissue, which consists of meristematic cells containing dense cytoplasm and swollen nuclei (Figs. 2*E*, 2*I*).

Fig. 1 Three bud physiological statuses in the first node [*A*, dormancy shoot bud (DSB)] and the second node [*B*, activity shoot bud (ASB) and *C*, ramet leave bud (RLB)] of strawberry stolon. The scale bar in the figure showing whole strawberry stolon is 1 cm, and in the other figures is 1 mm.

Fig. 2 Slice observation of strawberry stolon. (*A*) Growth arrest in the first node and its stepping into dormancy, (*B*) Continuous development as a new stolon branch upon dormancy release. (*C*) Arrows indicate the trifoliolate ramet leave buds in the second node. (*D*) Vascular bundles (arrow) of the new developing stolon in the second node connected to the primary stolon. (*E*) The tissues from the outside to the inside of the stolon are epidermal hair (purple) and epidermis (orange), thick cortex (red), cambium (green; composed a large number of parenchymatous cells), phloem (blue), xylem (grey), and pith (black). (*F–G*) vascular of the lateral buds on the first (*F*, orange arrow) and second nodes (*G*, orange arrow) of the strawberry stolon were connected inward with the primary stolon vascular. (*H-I*) adventitious root primordia, which originated from the cambium. The scale bar is 0.5 mm in figures *A-B* and *F-I*, 1 mm in figure *C-D*, and 0.3 mm in figure *E*.

Stereoscopic and SEM observation of developing stolon buds

Dormancy bud in the first node––In order to acquire more details on the developmental characteristics of the first and the second node buds of the strawberry stolon, different developmental phases of the stolon buds were observed under the stereomicroscope and scanning electron microscope (SEM), respectively. We observed that in the early stage of stolon elongation (when the stolon length was 4–10 cm), the buds on the first node of the stolon grew with the respective development of the stolon at the early stage (Figs. 3 *A–C*). For example, when stolon was 4 cm in length, a very tiny growing point located in the center of a trifoliolate bud could be seen after the outermost bract was peeled off from the first node (Fig. 3*A*). Continually, with the growth of stolon (when the stolon length was 6–7 cm), the top trifoliolate leaf bud on the first node developed further, and the growth point at the central base of the buds also grew (Figs. 3*B–C*). With the further elongation of the primary stolon, when the stolon length was 8–9 cm, the bud of the original trifoliolate gradually developed into a young trifoliolate bract and was densely covered with trichomes (Figs. 3*D–E*). When this young trifoliolate was peeled off sequentially, another tightly closed thin trifoliolate bud could be seen (Fig. 3*F*), and for protecting the underneath growing point. This is the landmark when the bud of the first node in the strawberry stolon ceases to develop and enters into dormancy; therefore, when we observed continually with the primary stolon elongated further, this thin trifoliolate bud structure showed no change. Our conclusion was further confirmed by the magnified observation of SEM, that is, the first trifoliolate bud under the bract of the first node continuously develops into a young trifoliate, with the development of the primary stolon at an early stage of stolon development or elongation (Figs. 3*G*, 3*J*). Similarly, when this young trifoliolate leaf was peeled off, the structure of the thin, tightly closed trifoliolate bract was visible (Fig. 3*J*). With all this, the outermost new trifoliolate leaf bud and the inner growing point ceased to develop, and showed no further development as the primary stolon elongated continually, indicating its stepping into a state of dormancy.

Fig. 3 Dormancy shoot bud (DSB) developmental phases in the first node. (*A–C*) Three typical developmental phases of DSB (arrow) at the early stage of primary stolon elongation. (*D–E*) DSB covered by a young trifoliolate leaf bract.(*F*) closed bract with a DSB inside. (*G–J*) scanning electron microscope (SEM) photomicrographs of DSB in A–C and F. The scale bar is 10 μm in A, 25 μm in B, 50 μm in C, 100 μm in D–E, 150 μm in F, 10 μm in G–H, and 20 μm in I–J.

Activity shoot bud in the second node––The active stolon bud (ASB) under the outermost bract of the second node of a strawberry stolon is quite different from the DSB located in the first node, showing an active development state in the whole process of primary stolon development (Fig. 4). The developmental process of ASB inside the second node was also showed that the trifoliolate leaf bud developed firstly (Figs. 4*A–D*). When this trifoliolate leaf bud developed into a young trifoliolate (Fig. 4*E*), the new inner trifoliolate could be seen (Fig. 4*F*), and at the same time, a new growth point near the trifoliolate cluster started to develop (Fig. 4*F*). The results of SEM observation showed further details of the development of trifoliolate leaf buds, which exhibited a high developmental activity (Figs. 4*G–I*).

Fig. 4 Activity shoot bud (ASB) development in the second node. (*A–B*) ASB primordium located at the center of the developing and matured bract. (*C–E*) ASB apex development when the matured bract was peeled off. (*F*) ASB structure when the young apex of ASB was peeled off again and a new growth point (arrow). (*G–I*) are the respective SEM observations for *D–F*; in these figures, we know the trifoliolate apex exhibited a high developmental activity. The scale bar is 50 μm in *A-D*, 100 μm in *E–F*, and 20 μm in *G–I*.

Ramet buds in the second node– –Unlike the axillary development of DSBs and ASBs, the developmental process of the strawberry ramet leaf bud (RLB) is relatively simple and rapid (Fig. 5). The apical region of a strawberry stolon contains multiple leaf bud primordia; when one leaf primordium gradually develops into a young trifoliolate, the next leaf primordium is initiated out as a visible developing trifoliolate (Figs. 5*A*, 5*B*), and then each leaf primordium develops into a young leaf, orderly, to formed a young leaf cluster (Figs. 5*C–F*). The developing activity stolon branch is located laterally to these leaf clusters (Figs. 5*E*, 5*F*). The SEM observation showed that the trifoliolate bract firstly grown out is located at the top of each trifoliolate primordium to protect the inner part (Fig. 5*G*). Each trifoliolate bract was tightly connected with each other in a complementary manner (Fig. 5*G*) to save the limited growth space. As a result, each connected young trifoliolate in the ramet of the second node is well positioned, and the active stolon bud is located adjacently (Figs. 5*I*, 5*J*).

Fig. 5 Ramet leave bud (RLB) development in the second node of a strawberry stolon. (*A*) Pure trifoliolate leave enclosed in the bract. (*B*) Newly formed bract, with a new primordium of trifoliolate leaves inside. (*C–E*)show the development of ramet leave buds and laterally located newly formed stolon buds. (*F*) young trifoliolate cluster and laterally located new stolon in the second node. (*G* and *H*) detailed exhibition of ramet leave buds cluster and the bird's eye perspective of a single developing leaf bud, respectively. (*I–J*) show the development of laterally located newly formed stolon buds with the growth of apical ramet buds. The scale bar is 150 μm in *A–B* and *D–E*,300 μmin *C* and *F*, 100 μmin *G*, 10 μmin *H*, and 20 μm in *I–J*.

Protein profiles among different strawberry stolon buds

For searching the regulatory factors in modulating the heterogeneity of strawberry stolon buds at the proteomic level, the DEPs from different types of buds were assessed by profiling the proteome using the TMT labeling system. The expression profiles of the proteins extracted from DSBs (labeled with 126, 127N, 127C), ASBs (labeled with 128N, 128C, 129N), and RLBs (labeled with 129C, 130N,130C) on a 10-cm long strawberry stolon were analyzed.

LC-MS/MS– –A total of 42,737 peptide fragments, among which 26,135 were unique peptides corresponding to totally 7,271 proteins (Fig. 6*A*), were assessed by TMT–based LC-MS/MS mass spectrometry identification and a search against the Uniprot_mouse_76417 database employing MASCOT engine integrated with Proteome Discoverer 1.4 software (supplemental Table S1, S2). A 1.2-fold-change cut-off with P-value<0.05 was used to indicate significant changes in the abundance of DEPs among different strawberry stolon buds (supplemental Fig. S2). By analyzing the quality control data, we found that the TMT results that were achieved by using high-quality Q Exactive mass spectrometer was reliable. The accuracy and high resolution in this experiment can maintain good quality deviation in the process of data acquisition, and finally obtain the high-quality spectrograms of MS1 and MS2. The quality deviation of all identified peptides was mainly within 10 ppm (supplemental Fig. S3), indicating that the identification results were accurate and reliable. When the rigid analyzing tool of MASCOT (FDR<0.01) was used for judging each MS2 spectrogram, we obtained an ideal score with a median of 34.06, and more than 86.21% peptides scored higher than 20 (supplemental Fig. S4). The protein ratio (approximately 1.0) distribution of the three groups (ASB/DSB, RLB/DSB, and RLB/ASB) are shown in supplemental Fig. S5.

Features of identified proteins– –The distribution of unique peptides defining each protein is shown in Figure 6*B*, with over 61% of them, including at least two unique peptides (supplemental Table S1). The average molecular mass of the identified gene products ranged from 10 to 70 kDa (Fig. 6*C*). The distribution of t (PI) of the identified proteins was mainly in the area of 5.0–10.0, with most PIs ranging from 6.0 to 7.0 (supplemental Fig. S6). Comparisons between the DSB, ASB, and RLB groups led to the identification of altogether 1,307 (ASB/DSB, including 691 up-regulated and 616 down-regulated), 363 (RLB/DSB, 168 up-regulated and 195 down- regulated) and 626 (RLB/ASB, 256 up-regulated and 370 down-regulated) DEPs

(supplemental Table S3). The variation of the three biological replicates of each group (DSB, ASB, and RLB) was calculated according to their quantitative data, with most proteins exhibiting less than 20% variation (supplemental Fig. S7), indicating the high quality and repeatability of data.

Fig. 6 Results of the tandem mass tags (TMT)–based liquid chromatography-tandem mass spectrometry (LC-MS/MS) identification of the stolon buds of the Ning Yu variety of strawberry. (*A*) The classification of the items used in identifying proteins; (*B*) Number of unique peptides that were matched to each identified protein; (*C*) Distribution of the average molecular mass of identified proteins.

Common DEPs between groups– – According to the fold changes in each group (supplemental Table S3), we selected out top 10 up- and down-regulated DEPs between groups for further analyzing (Table 1). By further selecting the common DEPs in these 10 up- or down-regulated proteins (supplemental Table S4), we found that all five common proteins between the groups of ASB/DSB and RLB/DSB were down-regulated DEPs. These five common proteins, including cucumisin-like, serine carboxypeptidase-like 27, ornithine decarboxylase-like, 36.4 kDa proline-rich protein, and ribulose bisphosphate carboxylase small chain, chloroplastic-like protein are mainly involved in stimulating the developmental phases or promoting the dormancy process of the first node of DSB in a strawberry stolon. Between the groups of RLB/DSB and RLB/ASB, only one up-regulated common DEP of pentatricopeptide repeat-containing protein was found. Six common DEPs were identified between the groups of ASB/DSB and RLB/ASB, and all DEPs showed consistent up-regulated expression in ASB/DSB and down-regulated expression in RLB/ASB. These six common DEPs in the ASB/DSB and RLB/ASB groups were fasciclin-like arabinogalactan protein 12 (double), glucuronoxylan 4-O-methyltransferase 3-like, aquaporin TIP2-1, putative 4-hydroxy-4-methyl-2-oxoglutarate aldolase 2, and fruit protein pKIWI501-like. Thus, all these six common DEPs were highly expressed in ASBs, when compared with DSBs and RLBs, suggesting they are strongly functional in the ASB developmental process. In addition, three common proteins were found in all three groups; they were hypothetical protein CARUB_v10021660mg, blue copper protein-like, and glycine-rich cell wall structural protein, with the same expression modes of ASB/DSB-up, RLB/DSB-up, and RLB/ASB-down. This implies that these three proteins have the ability to promote the entry of DSBs into dormancy and to stimulate the development of ASBs at the same time. The other DEPs among the top 10 up- or down-regulated proteins are specifically expressed in each group (supplemental Table S5).

Table 1. *Top 10 of up- and down-regulated differentially expressed proteins between groups*

Additional large-scale analysis of DEPs between groups of co-up and co-down regulation was also carried out, as shown in the Venn diagram of Figure 7 (detailed information in supplemental Table S6, S7, S8). We found that no DEP showed co-up regulation; only one DEP of GDSL esterase/lipase showed co-down regulated mode among all three groups (Fig. 7*A*, 7*B*). When the co-up plus co-down regulated proteins were counted at the same time, there are 45 common-DEPs in all three groups (Fig. 7*C*). Among all statistics, one group of data showed special performance, that is, ASB/DSB and RLB/ASB have almost no co-up or co-down proteins (Fig. 7*A*, 7*B*) separately, but when we counted all total co-up plus co-down DEPs, 407 common DEPs appeared in both ASB/DSB and RLB/ASB groups, simultaneously (Fig. 7*C*). These results indicated that each of the 407 DEPs shared common down-regulated or up-regulated expression patterns in the groups of DSB and RLB when compared with ASB, further suggesting that all these proteins have dual functions in stimulating the RLB formation while promoting the stepping of DSBs into dormancy, but have an antagonistic effect on the ASB development in strawberry stolon, simultaneously. Thus, exploring the regulatory mechanisms of these 407 DEPs is of great significance to clarify the dormancy of the first node DSBs and the formation of the second node RLBs.

Fig. 7 Venn diagram of DEPs that have Co-up (*A*) and co-down (*B*), as well as total co-up plus co-down (*C*) expressions from each experimental group comparison.

Bioinformatics analysis

All DEPs detected by MS were subjected to a bioinformatics analysis for further classification.

Cluster Analysis– –The hierarchical clustering results were expressed as a respective heat map (Fig. 8). The *X*- and *Y*-coordinates represented sample and differentially expressed proteins, respectively. As determined by a horizontal comparison, the samples could be classified into three categories: DSB, ASB, and RLB. Such a classification was associated with high accuracy, suggesting that the selected DEPs could effectively distinguish between samples. Furthermore, a vertical comparison indicated that the selected proteins could be classified into two categories with opposite directional variation, which displayed the expression patterns of DEPs in three groups (supplemental Fig. S8), demonstrating the rationality of the selected DEPs. The cluster analysis, thus, supported that the DEPs screened out in this experiment were reasonable and accurate.

Fig. 8 Cluster analysis of differentially expressed proteins. Through horizontal comparison, samples could be classified into three categories, suggesting that the selected DEPs could effectively distinguish between samples. A vertical comparison indicated that proteins could be classified into two categories with opposite directional variation, demonstrating the rationality of the selected DEPs. M, N, and D represent the DSB, ASB, and RLB groups, respectively. (*A*) is DSB/ASB, (*B*) is RLB/DSB, and (*C*) is RLB/ASB.

GO Functional Annotation and Analysis– –The DEPs (1,307, 363, and 626) between ASB and DSB, RLB and DSB, and RLB and ASB groups corresponded to 1,931, 1,194, and 1,276 functional annotations, respectively (supplemental Table S9-11). The DEPs were individually analyzed against the Gene Ontology (GO) database using three sets of ontologies: biological process, molecular function, and cellular component (Fig. 9). The analysis showed that among all three groups of ASB/DSB, RLB/DSB, and RLB/ASB, numerous DEPs could be classified in the same GO category (supplemental Table S9-11). The top two common*biological process*categories were metabolic process (over 35%) and cellular process (over 25%). The top four common *molecular function* categories were catalytic activity (over 35%), binding (over 25%), transporter activity, and structural molecule activity. The top four common *cellular component* categories were cell (over 25%), cell part (over 25%), organelle (over 15%), and membrane proteins (over 15%). A small number of other DEPs existed in cellular component categories, including membrane part, organelle part, and macromolecular complex, with the ratio of approximately 10%.

For further exhibition of top 20 enriched GO terms (supplemental Fig. S9), we know detailed information of functional proteins in *biological process* (*BP*) of ASB/DSB were oxidation-reduction process (~100 DEPs) and regulation of RNA metabolic process (supplemental Fig. S9*A*), in RLB/DSB, they were DNA metabolic process and photosynthesis, with the same number of DEPs (14), as well as DNA conformation change and replication (supplemental Fig. S9*B*), whereas for RLB/ASB (supplemental Fig. S9*C*), there were small numbers of DEPs, which were classified into the secondary metabolic process, one-carbon metabolic process, secondary metabolite biosynthetic process, and phenylpropanoid metabolic process.

Molecular function (*MF*) analysis showed that the GO terms in ASB/DSB were catalytic activity (~450 DEPs) and oxidoreductase activity (over 100 DEPs), as well as DNA binding (supplemental Fig. S9*A*). In RLB/DSB, the MF proteins were DNA binding and helicase activity (supplemental Fig. S9*B*). In the RLB/ASB MF GO terms, a large numbers DEPs belonged to catalytic activity (~250) and oxidoreductase activity (~60) and protein dimerization activity (supplemental Fig. S9*C*).

The *cellular component* (*CC*) terms in ASB/DSB were thylakoid and thylakoid part and chromatin. Combining the GO terms identified in the MF and BP analysis above, we found that the differences existed mainly at the RNA level (supplemental Fig. S9*A*). Between the groups of RLB and DSB, the GO terms were thylakoid (22), thylakoid part (16), plastid thylakoid (14), chloroplast thylakoid (14), photosynthetic membrane (14), and thylakoid membrane (12) (supplemental Fig. S9*B*). This suggested that their differences between RLB and DSB mainly occurred in their capacity of photosynthesis. In RLB/ASB, all DEPs of CC were functional compartment of chromosome- or DNA-relative proteins, and showed a coincidence trend of low number (supplemental Fig. S9C).

Fig. 9 Gene ontology annotation of differentially expressed proteins (DEPs) among groups. The *X*-axis represents the Gene Ontology functional classification. The main *Y*-axis represents the number of DEPs, and the secondary *Y*-axis represents the classified DEP ratio in respective group's total DEPs (ASB/DSB, RLB/DSB and RLB/ASB). *A*, Biological process. *B*, Molecular function. *C*, Cellular component.

KEGG Pathway Analysis—By searching the major biological pathways and relevant regulatory processes involved in the Kyoto Encyclopedia of Genes and Genomes (KEGG), we analyzed all DEPs among groups (Fig. 10). The results indicated that the spliceosome (43 DEPs, as shown below) and ribosome (29) had high enrichment between ASB and DSB (Fig. 10*A*, supplemental Table S12). This suggested that the differences in transcription or translation are thefundamental reason for the difference between ASB and DSB. As for RLB/DSB (Fig. 10*B*, supplemental Table S13), the photosynthesis (13) pathway is the highest enrichment of DEPs. This is an additional proof of the fact that the main RLB function is photosynthesis for the next clonal generation of ramets. In addition, two highly enriched pathways of DNA replication and spliceosome still existed, indicating that both genetic and transcriptional level differences existed between RLB and DSB. The participation of DEPs in the phenylpropanoid biosynthesis pathway (18), as well as in carbon metabolism relative pathways, such as starch and sucrose metabolism (15), amino sugar and nucleotide sugar metabolism (14), and glycolysis/gluconeogenesis (11), showed high enrichment between groups RLB and ASB (Fig. 10*C*, supplemental Table S14). This indicated that phenylpropaniod biosynthesis worked for differentiation between RLBs and ASBs in the second node of strawberry stolon, especially for the formation of vessels during the ASB developmental processes, as discussed below.

Fig. 10 KEGG Pathway Analysis between different groups of ASB/DSB (*A*), RLB/DSB (*B*), and RLB/ASB (*C*).

PPI (Protein-Protein Interaction) *Analysis*––We used the PPI database and relevant literature to confirm the interactions of the identified proteins or DEPs, as well as of other proteins that interacted directly with them. Construction of a PPI network (supplemental Table S15), which was expressed as nodes and links, contributed to extracting effective protein information from various points of view and obtaining comprehensive information that could not be obtained through the analysis of only a single protein (Fig. 11). According to the results, 20 high-connectivity degree DEPs, with a degree value of more than 30, were selected out between groups ASB and DSB (Table 2). Six and 11 DEPs, with connectivity degrees higher than 10, were selected from the RLB/DSB and RLB/ASB groups, respectively (Table 2). The results of this part are highly consistent with those of KEGG, which indicated that the difference between ASB and DSB was mainly due to the difference at the transcriptional level, while the difference between RLB and DSB was mainly due to the difference at the genetic level. For further showing the direct protein-protein relationship, we selected four typical DEPs of NADH-GOGAT & GDH, PK, MCM 2–4 and 6–7 as the PPI core (Fig. 11A–C). In additional, we drew the PPIs in the phenylpropanoid biosynthesis pathway (Fig. 11D) to further clarify the key protein-protein interactions.

Table 2 *DEPs with high connectivity degree in PPI analysis between groups*

Fig. 11 Protein-protein interaction (PPI) of the core proteins NADH-GOGAT, GDH (*A*) and PK (*B*), MCM 2-4 and 6-7 (*C*), as well as phenylpropanoid biosynthesis pathway (*D*).

Abbreviations: *A*, vesicle-associated protein 2-2-like (V-AP 2-2), putative formamidase C869.04 isoform X1 (PF), probable aquaporin PIP-type 7a (A-PIP 7a), phosphoenolpyruvate carboxylase 2 (PC 2), malate dehydrogenase, glyoxysomal isoform X2 (MDGI), glycine cleavage system H protein 3, mitochondrial-like (GCH 3), glycine cleavage system H protein 2, mitochondrial (GCH 2), glutamine synthetase cytosolic isozyme (GSCI), glutamate synthase 1 [NADH], chloroplastic isoform X1 (NADH-GOGAT), glutamate dehydrogenase 1 (GDH), glutamate decarboxylase 4-like (GD 4), bifunctional 3-dehydroquinate dehydratase/shikimate dehydrogenase, chloroplastic-like (SD), aquaporin TIP4-1 (A-TIP4-1), aquaporin TIP2-1 (A-TIP2-1), aminomethyltransferase, mitochondrial (AM) , aldehyde dehydrogenase family 3 member H1-like (ADF 3H1), aldehyde dehydrogenase family 3 member F1 (ADF 3F1), acetyl-CoA carboxylase 1-like isoform X1 (A-Co1 C1), allantoinase (ALT); *B*, uncharacterized protein LOC105350465 (LOC105350465), transketolase, chloroplastic (TK), pyruvate kinase, cytosolic isozyme (PK), pyruvate decarboxylase 2 (PD 2), pyrophosphate-fructose 6-phosphate 1-phosphotransferase subunit alpha (PF6-P), probable DNA primase large subunit (DNA-PLS), polyribonucleotide nucleotidyltransferase 2, mitochondrial (PBNT 2), phosphoglycerate kinase, cytosolic-like (PKC), phosphoenolpyruvate carboxylase 2 (PC 2), nucleoside diphosphate kinase 3-like (NDK 3), NADP-dependent malic enzyme (NADP-DME), NADP-dependent glyceraldehyde-3-phosphate dehydrogenase (NADP-DG 3PD), NAD-dependent malic enzyme 59 kDa isoform, mitochondrial (NAD-DME), L-lactate dehydrogenase A (L-LD), glyceraldehyde-3-phosphate dehydrogenase GAPCP1 (G3PD GAPCP1), glyceraldehyde-3-phosphate dehydrogenase B, chloroplastic (G3PD B), glyceraldehyde-3-phosphate dehydrogenase A, chloroplastic (G3PD A), glucose-6-phosphate

isomerase 1, chloroplastic (G6PI), glucose-6-phosphate 1-dehydrogenase, cytoplasmic isoform 2 (G6P1D), fructose-bisphosphate aldolase 1, chloroplastic (FBA 1), DNA-directed RNA polymerases IV and V subunit 4 isoform X2 (DNA-RNA P IV), DNA-directed RNA polymerases II, IV and V subunit 11 (DNA-RNA P II), DNA-directed RNA polymerase V subunit 5A-like (DNA-RNA P V), DNA-directed RNA polymerase III subunit rpc4 isoform X1 (DNA-RNA P III), DNA polymerase epsilon subunit 3 (DNA-PE), DNA polymerase epsilon catalytic subunit A-like isoform X2 (DNA-PEC), DNA polymerase delta catalytic subunit (DNA-PDC), DNA polymerase alpha subunit B (DNA-PA), cytosolic enolase 3 (CE 3), ATP-dependent 6-phosphofructokinase 6 (ATP-D6P6), 2-isopropylmalate synthase 1, chloroplastic-like (2-IS1); *C*, DNA replication licensing factor MCM 2-4 and 6-7, probable DNA primase large subunit (DNA-PLS), structural maintenance of chromosomes protein 4-like (SMCP4), structural maintenance of chromosomes protein 2-1-like (SMCP2), replication factor C subunit 1 (RFCS1), structural maintenance of chromosomes protein 3 (SMCP3), histone H3.3 isoform X1 (H-H3I), hypothetical protein CARUB_v10021660mg (CARUB), DNA ligase 1-like isoform X2 (DNA-L 1IX2), DNA polymerase delta catalytic subunit (DNA-PDCS), DNA polymerase alpha subunit B (DNA-PASB); *D*, phenylalanine ammonia-lyase 1 (PAL1), caffeoylshikimate esterase (CSE), cytochrome P450 98A2 (P450-98A2), cinnamoyl-CoA reductase 1-like (CCR1-like), trans-cinnamate 4-monooxygenase (TC4M), 4-coumarate-CoA ligase 2-like (C4L-like), cytochrome P450 84A1 (P450-84A1), beta-glucosidase 44-like (BG-44-like), beta-glucosidase 42 (BG-42), probable cinnamyl alcohol dehydrogenase 9 (CAD9), peroxidase 17-like (POD 17-like), caffeic acid 3-O-methyltransferase (COMT), probable cinnamyl alcohol dehydrogenase 1 (CAD1), caffeoyl-CoA O-methyltransferase (CCOMT).

PRM (Parallel Reaction Monitoring) verification

To further verify the results of MS, three DEPs (Pyruvate Kinase (PK), MCM2, and PAL1) were selected for PRM analysis (Fig. 12). The screening criteria were formulated based on the following two principles: 1) proteins with potential biological functions and peptide fragments greater than 1, as identified by LC-MS/MS; and 2) proteins that were specifically expressed in one group of buds when compared with the other two groups of buds and have not been reported yet.

The results of the LC-PRM/MS analysis performed on 12 peptide fragments of three target proteins from three groups of strawberry samples showed that the quantitative information of target peptide fragments could be obtained in all nine samples. Subsequently, the relative quantitative analysis was carried out on target peptide fragments and proteins through the incorporation of heavy isotope-labeled peptide fragments. The results indicated that of the three target proteins, the expression quantities of PK and PAL1 in the ASB group were markedly upregulated compared with the DSB and RLB groups; whereas the expression quantity of MCM2 in the RLB group was significantly up-regulated compared with that in the DSB and ASB groups, additionally verifying the facticity and accuracy of the TMT method in this study.

Fig. 12 PRM verification of the expression quantities of target proteins PK, MCM2, and PAL1. DSB: dormancy shoot bud; ASB: activity shoot bud; RLB: ramet leaf bud; PK: pyruvate kinase; MCM2: minichromosome maintenance protein 2; PAL1: phenylalanine ammonia-lyase 1.

Data are means and standard errors, of 3 groups of each type bud, and the experiment was repeated 3 times. Different letters in the same index means the significant difference among buds, separately ($P<0.05$). Bars represent the standard deviation ($n=3$).

Discussion

Heterogeneity among the buds of different stolon nodes

Stolon is an asexual reproductive organ of strawberry. It is important to study the development process of the buds at different nodes for strawberry production. The stolon of the octoploid cultivated strawberry (*F.* × *ananassa* Duch.) consists of two nodes—the first node usually remains in dormancy, and the second node has the ability to form the ramet (Fig. 1) (4). A new stolon is usually originated from the axillary bud inside the first leaf of the ramet, where the bud is mostly conducive to absorbing water and nutrients, and is, therefore, most likely to develop as a new stolon branch[16]. The colonizing behavior

and functional morphology of stolons (Fig. 2) indicate that ramet survival, prior to rooting, is achieved through the plasticity of intra-stolon ramet competition for resources such as water, ions, and photoassimilates[7].

By observing the buds on the nodes, we found that the buds on the first node developed into a certain stage and then ceased development at the early phase of the primary stolon elongation, indicating their entry into dormancy (Fig. 2, 3). Furthermore, under favorable conditions, the buds of the first node can sprout out as another stolon branches, but these new stolon branches are usually much smaller and thinner than the primary stolon (Fig. 2*B*). If the tip of the stolon is removed, the first node can develop into a ramet rather than a stolon branch[4], indicating that the bud in the first node has the binary functions of forming a new stolon branch or an independent ramet simultaneously, given that it might be an undifferentiated bud or has the ability to dedifferentiate again. However, under normal conditions, the factors that regulate the ceasing of the first node bud development and its entry into dormancy are still unknown. We can elaborate the possible factors by comparing the former studies on the key regulators of axillary bud growth and dormancy. The shoot branching process generally involves two developmental stages: the formation of axillary meristems in the leaf axils and the growth of axillary buds[17]. In many plant species, the growth of axillary meristems is inhibited by the primary shoot or primary inflorescence[18]. This phenomenon is generally known as apical dominance. The plant hormones auxin and cytokinin are thought to have a major role in controlling this process[19]. Auxin has an inhibitory effect on the growth of axillary buds, whereas cytokinin promotes axillary bud outgrowth. The mechanisms of axillary bud outgrowth depend on the ratio of these two hormones rather than the absolute levels of either hormone. In other plants, the axillary meristems might initiate a few leaves and then become developmentally arrested or dormant because the terminal bud inhibits the growth of axillary buds to grow predominantly[17]. As for strawberry, we suggest that the first node bud development on stolon belong to this type of axillary growth, and we observed that axillary meristems initiated a few trifoliolate bracts, as shown in Figure 2, followed by ceased development and entry into dormancy. Consistent with the previous studies, the arrested development of axillary buds in the first node of strawberry and their stepping into dormancy might be comprehensively caused by environmental factors and a feedback to apical dominance. Thus, according to our observation, this dormancy could be released under suitable environment and growth could be resumes to develop into a new branch of stolon (Fig. 2*B*). It is possible that a set of genes or proteins that controls the outgrowth or dormancy of axillary buds acts at different phases of the bud developmental processes. This type of molecular study might provide the basis for understanding the regulation of dormant or outgrowing axillary buds in strawberry stolon nodes.

Proteomics for analyzing different stolon buds

Comparative proteomics is a useful approach for identifying functional proteins in illustrating the developmental regulation mechanism of plants[20-23]. Recently, with the tremendous release of the plant reference genome data, more and more comparative proteomics approaches have been applied for studying bud heterogeneity in crops[11-14]. Previous studies compared the proteomes of the first and second nodes of the strawberry stolon to elucidate the internode differences, and found that the DEPs were mostly related to photosynthesis[10]. This study was useful for understanding the heterogeneity of stolon buds in strawberry, but it still requires further investigation. On one hand, the second node of strawberry stolon contains not only a single type of bud, but two types of buds, RLB and ASB; thus, it is necessary to anatomically separate the second node into two different types of buds before analyzing them. As mentioned above, DSB, ASB and RLB on the same stolon were separated and categorized into three types of bud groups, with each group having three biological repeats, and each repeat containing 200 buds, before performing the TMT analysis. Approximately 540 fresh stolons, which were in the same growth phase, were anatomically dissected and their DSBs, ASBs, and RLBs were collected as independent samples for experiments in order to fully shield the differences among the experimental individuals and ensure the reliability of the experimental data. In addition, the TMT method is more accurate than the traditional two-dimensional gel electrophoresis in isolating DEPs, and can successfully identify DEPs with low expression levels among groups[15]. Therefore, we used the TMT method to explore the primary causes leading to the differences between DSB and ASB, which existed as the stolon axillary shoot buds, but under quite different physiological conditions. In addition, we firstly determined the factors regulating bud differentiation between RLB and ASB, which are commonly located on the second node of a strawberry stolon. It further investigation to

elucidate the reason underlying the development of an axillary ASB from a newly formed ramet, which mainly originates from an RLB and then further develops into an elongated stolon.

TMT revealed the heterogeneity of stolon buds in strawberry

The proteome has an important characteristic difference with the genome, that is, proteins have a direct influence on each other[24]. The realization of the function of a protein usually depends on its interaction with other proteins implying that no independent functional protein exists[25-27]. Therefore, through comprehensive analysis and evaluation of GO annotation (BP, MF, CC), enrichment in KEGG, and connective degree in PPI, we can predict the core functional DEPs involved in the key metabolic pathways[26, 28].

Between ASB and DSB– –According to the comprehensive analysis between GO and KEGG, we know that the difference at the transcriptional level might lead to the differences in their physiological statuses. On combining the PPI analysis, the DEP of splicing factor 3A subunit 2 isoform X1 showed a higher connectivity degree value of 42. As previous studies reported that alternative splicing has a wide influence on the evolution of the complex networks of the regulation of gene expression and variation in contribution to the adaptation of plants to their environment and, therefore, will impact the strategies for improving plant and crop phenotypes, such as entry into dormancy under stress conditions[29, 30]. Splicing factor (SF), as a positive contributor in the process of alternative splicing, recruits splicing-related proteins and confirms the splicing position and spliceosome assembly, and then participates in the morphological determination of plant organs[31]. SF mainly contained two families of proteins—Ser/Arg-rich (SR) and heterogeneous nuclear ribonucleoprotein particle (hnRNP). In our PPI analysis, of the 19 DEPs, which had high connectivity degree values of more than 30, four (21%) were SRs and six (32%) were hnRNPs. Thus, we suggest that these high connectivity degree SRs and hnRNPs might act as crucial factors in regulating the morphological determination of the heterogeneity of the stolon axillary ASBs and DSBs (Fig. 13)

Fig. 13 Possible mechanisms for differentially expressed proteins in regulating the heterogeneity of stolon buds in strawberry.

Similarly, we should also pay attention to the other two DEPs of pyruvate kinase, cytosolic isozyme (degree 33) and uncharacterized RNA-binding protein C1827.05c (degree 31). Pyruvate kinase (PK) has been well studied in modulating bud dormancy or bud break in pomology, and the activity of PK has been found to be lower in dormant buds than in non-dormant buds and peaked in the green tip stage just before the start of rapid expansion and declined thereafter[32-34]. In our study, PK, cytosolic isozyme（degree 33）is also another highly connective DEP with high expression quantity in ASB, but is expressed at relatively low levels in DSB and RLB (Fig. 12), suggesting that this pyruvate kinase, cytosolic isozyme functions mainly in ASB than in DSB and RLB (Fig. 12). This was consistent to a previous study, but elucidation of the detailed functional mechanism still needs further investigation.

In eukaryotes, RNA-binding proteins (RBPs) play crucial roles in all aspects of post-transcriptional gene regulation. They regulate diverse developmental processes by modulating the expression of specific transcripts. Clearly, they function by regulating pre-mRNA splicing, polyadenylation, RNA stability, and RNA export, as well as by influencing chromatin modification[29]. Uncharacterized RNA-binding protein C1827.05c (degree31), as a special DEP with relatively high fold change between groups ASB and DSB, might co-function with the splicing factors and ribosomal proteins (Fig. 13, supplemental Table S15).

Between RLB/DSB– –The differences between RLB and DSB mainly focus on the DEPs involved in photosynthesis (Fig. 9–10); this might be caused by the difference at gene duplication level. We identified four DNA replication licensing factors minichromosome maintenance (MCM) 2, 3, 4, and 7 from a total of six high-connectivity degree (>10) DEPs (supplemental Table S15), The DNA replication licensing factor MCM complex, consisting of six subunits, MCM 2–7, is loaded onto the replication origins through loading factors (origin recognition complex [ORC], Cdc6, and Cdt1) and forms an MCM double hexamer that licenses the initiation of DNA replication[35]. The functions of MCM have been mainly studied in medical science, especially in cancer[36]. Here, we suppose that MCM 2, 3, 4, and 7 might upregulate the expression of photosynthetic

genes and indirectly regulate photosynthesis substance allocation and transportation by modulating DNA replication or endoreduplication. This was consistent with the previous studies, which reported that the parenchyma cells that store starch, sugar, and other substances in the fruits or seeds of plants reproduce through DNA replication or endoreduplication[37]. In order to verify the MCM expression mode in strawberry buds, we selected MCM2 as an identified protein and found that MCM2 showed a significantly high expression in RLB when compared with DSB and ASB (Fig. 12). Our hypothesis might also partially elucidate the findings of Atkinson et al. (2012), who reported that the hydraulic conductivity and polar auxin transport (PAT) pathway could determine hierarchical resource partitioning and ramet formation in *Fragaria* stolons (Fig. 13)[8].

The DEP with the highest fold change in expression between RLB and DSB was LIGHT-DEPENDENT SHORT HYPOCOTYLS (LSH) 10-like, with a fold change of 3.24 (Table I, supplemental Table S15). The LSH protein is an important functional regulator in modulating the plant shoot initiation process and could be used as a shoot marker in presaging the sites of shoot formation[38, 39]. LSH can be early expressed at the very early stage during zygotic embryogenesis in *Arabidopsis*[38]. As for strawberry, no studies have been conducted on short crown formation. Previous studies showed that differentiated organs can be converted to the other type of organs by various methods; for example, incubation in cytokinin-rich shoot induction medium converts the premature roots into shoots, particularly in those regions where the cytokinin receptor genes are up-regulated[40]. Flower-meristem-identity gene *LEAFY* is sufficient to determine the floral fate in lateral shoot meristems of both *Arabidopsis* and the heterologous species aspen, with the consequence that flower development is induced precociously[41]. In our study, the LSH 10-like protein was uniquely identified from among a total of 7,271 identified proteins by using high-throughput proteomics analysis between RLB/DSB. We speculate that the LSH 10-like protein should be involved in the degeneration of stolon apical meristem into RLBs (Fig. 13). Further studies are required to investigate on how LSH 10-like regulates the formation of a shorted crown of ramet and how ASB could be initiated from the position of a leaf axil in a newly formed ramet, and why the new-born secondary stolon (ASB formed) keep in continually running on the ground, instead of growing upward to the air.

Between RLB and ASB– –The differences between RLB and ASB in the second node are partially week compared to those between RLB and DSB. For example, glutamate synthase 1 [NADH], chloroplastic isoform X1 (connectivity degree 15, fold change 0.74, shortened as NADH-GOGAT 1) and glutamate dehydrogenase 1 (connectivity degree 12, fold change 2.05, shortened as GDH 1). NADH-GOGAT and GDH are important enzymes that participate in nitrogen metabolism by synthesizing glutamate[42]. The catalytic function of GDH was directly and more energy-efficient when compared to that of GOGAT[43, 44], and GDH mainly exists in non-photosynthetic tissues, such as root and early development cotyledons, of plants [45]. Unanimously, the fold change of NADH-GOGAT was higher than that of GDH between RLB and ASB.

Another group of special-feature DEPs could be found after a comprehensive analysis between RLBs and ASBs; they are the proteins involved in phenylpropanoid biosynthesis (Ko00940). According to previous reports, the multiple roles of phenylpropanoid biosynthesis in plant development are mainly focused on providing anthocyanins for pigmentation, flavonoids, such as flavones, for protection against UV photodamage, various flavonoid and isoflavonoid inducers of *Rhizobium* nodulation genes, polymeric lignin for structural support and assorted antimicrobial phytoalexins[46]. In particular, it plays an important role in the differentiation and development of lignin[47]. After comprehensively analyzing the KEGG pathways and PPIs, as well as fold change values among different groups, 18 DEPs highly related to the phenylpropanoid biosynthesis were selected out for further analysis (Fig. 11, supplemental Table S16). Among them, 15 DEPs were up-regulated in the group of ASB/DSB, whereas down-regulated in the RLB/ASB group simultaneously, and only three DEPs showed an opposite trend. In addition, almost all DEPs in the RLB/DSB group showed no significant difference in expression (Fold change 0.9–1.2). This means that most DEPs in the phenylpropanoid biosynthesis positively function in the formation process of ASB (Fig. 13). The DEPs of cinnamyl alcohol dehydrogenase 1 (CAD1) and phenylalanine ammonia-lyase 1 (PAL1) are only expressed in the RLB/ASB phenylpropanoid biosynthesis pathway. It has been reported that CAD1 and PAL1 are closely related to lignin synthesis[48, 49]. In addition, by determining the expression quantity of PAL1, we further confirmed that the target protein PAL1 was highly expressed in ASB, but showed low-level expression in DSB and RLB (Fig. 12). Based on that, we suggest that both of these two proteins might play important roles in the axillary bud specialization of a new ramet leaf into

ASB. We also speculated that they might play important roles in xylem differentiation or vascular formation when ASB developed into a new stolon (Fig. 13).

Conclusions

By combining the anatomical observation with the phenotypic observation and using proteomic networks with different types of strawberry stolon buds, we identified the definite dormancy phase of DSB and compared to the developmental differences among DSB, ASB, and RLB, as well as identified numerous protein signatures that translated to biological pathways and gene networks that might underlie the real reason of heterogeneity among different stolon buds in strawberry. The possible mechanisms for differentially expressed proteins in regulating the heterogeneity of stolon buds in strawberry were achieved (Fig. 13). The current study provides further information for understanding the heterogeneity of stolon buds in strawberry, as well as other fruit trees.

Materials And Methods

Experimental Design and Statistical Rationale

For tandem mass tags (TMT) labeling, each of the three TMT sets included three pooled control samples (n = 60 strawberry stolon buds in each sample) for across TMT-plex normalizations, as shown in Figure 1 (details below). The samples were randomized using an Excel function. The statistical tests used for each experiment are described within each section.

Plant material

The Ning Yu cultivar of cultivated strawberry (*Fragaria* × *ananassa* Duch.) was grown in the plastic tunnel of Plant Science Foundation in the Jiangsu Academy of Agricultural Sciences (32.22 °N, 118.52 °E), Nanjing, China, in April 2017. Three physiological statuses of buds in the first node (dormancy shoot bud) and the second node (including activity shoot bud and stolon apices) of a strawberry stolon were selected as materials (Fig. 1). The collected strawberry stolons had a length and diameter of 10 cm and 3 mm, respectively. Each type of bud sample was set as three replicates, with each replicate containing approximately 200 mg, which was collected from 60 buds. More than 540 fresh uniform stolons should be prepared for these three types of stolon buds as TMT samples. All material samples were collected as the youngest stolon buds (Figs. 1 A–C), immediately frozen in liquid nitrogen, and then stored at −80 °C for protein extraction. All three types of buds were used in triplicate samples for proteomics.

Phenotypic observation

In order to observe the morphological differences between the buds of the first and second nodes of the strawberry stolon, the bract of the young buds on the nodes should be peeled off using anatomical needles under the stereo microscope (Nikon SMZ 1500). For further observing the morphological differences among different types of stolon buds located on the first and second nodes, scanning electron microscopy (SEM) observation was used. For SEM observation, different types of stolon bud samples were dehydrated and fixed in 2.5% glutaraldehyde solution. For observing every detailed developmental morphological characteristic of the first and second node buds of the strawberry stolon, the stolon was sampled continuously from the beginning (2 cm stolon length and 2 mm diameter) of origination until the second node of the stolon formed an adventitious root primordium (30 cm length and 4 mm diameter). Approximately 20 different developmental phases of strawberry stolon were observed. The stereomicroscopic and SEM observations were all repeated 10 times for each developmental phase analysis. Finally, the most characteristically developed phase of stolon buds was determined and was sampled to be used in the next part of proteomics research.

Protein Extraction

Based on the anatomical and morphological changes of strawberry stolon buds (Figs. 2–5), three types of stolon buds, which were in the most characteristically developed phase, were chosen for quantitative proteomics analysis. Proteins were extracted from young buds using the tricarboxylic acid (TCA)/acetone precipitation and SDT cracking method according to the published protocol [50]. Briefly, approximately 200 mg stolon buds were grinded into a fine powder with liquid nitrogen and homogenized with five volumes of TCA/acetone (1:9). The sample was mixed with whirlpool and precipitated at −20 °C for more than 4 h, then centrifuged at 6,000 × *g* for 40 min at 4 °C, and the supernatant was discarded. The precipitated sample was washed thrice with cold acetone and then dried in ventilator. Subsequently, 20 to 30 mg dried powder was weighed and mixed with 30 volumes (m/v) of SDT cracking solution. The precipitate suspension was vortexed, kept in boiling water bath for 5 min, followed by ultrasonic crushing (80 w, 10 s, 15 s intermittent, 10 cycles), incubation in boiling water bath for 15 min, and centrifugation at 14,000 × *g* for 40 min. The protein concentration was determined using a bicinchoninic acid (BCA) protein assay (Bio-Rad, USA) kit according to the manufacturer's instructions. To confirm protein extraction, one-dimensional SDS-polyacrylamide agarose gel electrophoresis (PAGE) was performed (supplemental Fig. S1).

TMT analysis method

Protein Digestion and TMT Labeling

Protein digestion was performed according to the filter-aided sample preparation (FASP) procedure described by JR Wisniewski, A Zougman, N Nagaraj and M Mann [51], and the resulting peptide mixture was labeled using the 10-plex TMT reagent according to the manufacturer's instructions (Thermo Fisher Scientific). Briefly, each sample was dissolved, and 30 μL protein solution was mixed with DTT (1,4 dithiothreitol) to the final concentration of 100 mM, incubated in a boiling water bath for 5 min, and then cooled to room temperature. Thereafter, 200 μL urea (UA) buffer (8 M Urea, 150 mM TrisHCl, pH 8.0) was added and mixed evenly. The resulting solution was transferred to a 10-kD ultrafiltration centrifugation tube, centrifuged at 14,000 × *g* for 15 min, and discarded the filtrate (this step was repeated once). This was followed by the addition of 100 μL iodoacetamide (IAA) buffer (100 mM IAA in UA), oscillation at 600 rpm for 1 min, refractory reaction at room temperature for 30 min, and centrifugation at 14,000 × *g* for 15 min. Subsequently, 100 μL UA buffer was added and centrifuged again at 14,000 × *g* for 15 min; this step was repeated two times. Thereafter, 40 μL trypsin buffer [4 μg trypsin in 40 μL 100 mM triethylammonium bicarbonate (TEAB) buffer], was added and centrifuged at 14,000 × *g* for 15 min, and this step was repeated two times. When 40 μL trypsin buffer (4 μg trypsin in 40 μL 100 mM TEAB buffer) was added, oscillated at 600 rpm for 1 min, and placed at 37 °C for 16–18 h. A new collecting tube was replaced and centrifuged at 14,000 × *g* for 15 min. Thereafter, 100 mM TEAB buffer was diluted 10 times, and then 40 μL of the diluted TEAB buffer was added and centrifuged again at 14,000 × *g* for 15 min. The filtrate was collected, and the peptide segment was quantified (OD280).

For labeling, each TMT reagent was dissolved in 70 μL of ethanol and added to the respective peptide mixture. For each sample, 100 μg of the peptide mixture was labeled using the 10-plex TMT isobaric label reagent (Thermo Fisher Scientific) and then multiplexed and vacuum dried. All samples were labeled as (DSB-1)-126, (DSB-2)-127N, (DSB-3)-127C, (ASB-1)-128N, (ASB-2)-128C, (ASB-3)-129N, (RLB-1)-129C, (RLB-2)-130N, (RLB-3)-130C. A Pierce high-pH reverse-phase fractionation kit (Thermo Fisher Scientific) was employed to fractionate the TMT-labeled and digested samples into twelve fractions via increasing the acetonitrile step-gradient elution according to the manufacturer's instructions.

Mass spectrometry

Each fraction was injected for nano-liquid chromatography-tandem mass spectrometry (nano-LC-MS/MS) analysis. The peptide mixture was loaded onto a reverse-phase trap column (Thermo Scientific Acclaim PepMap100, 100 μm × 2 cm, nano Viper, C18) connected to a C18 reverse-phase analytical column (Thermo Scientific Easy Column, 10 cm long, 75 μm inner

diameter, 3 μm resin) in buffer A (0.1% formic acid) and separated with a linear gradient of buffer B (84% acetonitrile and 0.1% formic acid) at a flow rate of 300 nL/min, controlled by the IntelliFlow technology. The analysis gradient was a 1-h gradient consisting of 0–50% buffer B for 50 min, 50–100% buffer B for 5 min, and holding in 100% buffer B for 5 min.

The LC-MS/MS analysis was performed on a Q Exactive mass spectrometer (Thermo Fisher Scientific) coupled to an Easy-nLC system (Thermo Fisher Scientific) for 90 min. The mass spectrometer was operated in the positive ion mode. The MS data were acquired using a data-dependent top 10 method, dynamically choosing the most abundant precursor ions from the survey scan (300–1800 m/z) for high-energy collisional dissociation (HCD) fragmentation. The automatic gain control (AGC) target was set to 3E6 and the maximum injection time to 10 ms. The duration of dynamic exclusion was 40 s. The survey scans were acquired at a resolution of 70,000 at m/z 200; the resolution of the HCD spectra was set to 35,000 at 20,060; and the isolation width was 2 m/z. The normalized collision energy was 30 eV. The underfill ratio, which specifies the minimum percentage of the target value likely to be reached at the maximum fill time, was defined as 0.1%. The instrument was run with the peptide recognition mode enabled.

Data analysis

The MS/MS spectra output was obtained as a raw file and were searched using the Mascot engine (Matrix Science, London, UK; version 2.2) embedded into the Proteome Discoverer 1.4 (Proteome Discoverer Version 1.4., Thermo Fisher Scientific Inc. 2012) against the Uniprot_mouse_76417 database (76,417 protein sequences, downloaded on December 12, 2014) and the decoy database. For protein identification, the following options were used. Peptide mass tolerance=±20 ppm; MS/MS tolerance=0.1 Da; enzyme=trypsin; max missed cleavage=2; fixed modification: carbamidomethyl (C), TMT 10 plex (N-term), TMT 10 plex (K); variable modification: oxidation (M); false discovery rate (FDR) ≤ 0.01; protein quantification: the protein ratios are calculated as the median of only unique peptides of the protein; experimental bias: normalizes all peptide ratios by the median protein ratio, and the median protein ratio should be 1 after normalization.

Bioinformatics analysis

To determine the functional classification and biological properties of the selected differentially expressed proteins (DEPs), the identified protein sequences were mapped using the Gene Ontology (GO) terms. For this analysis, a homology search was performed for all transcript sequences localized in the diploid strawberry (*Fragaria vesca*) genome sequence[1] combined with the octoploid strawberry (*Fragaria* × *ananassa*) sequencing data[52], which were downloaded from the GDR database (https://www.rosaceae.org). Thereafter, all redundant sequences were removed from this combined dataset.

Gene Ontology and KEGG pathway annotation

The process of GO annotation by Blast2GO[53] can be roughly divided into four steps: sequence alignment (BLAST), GO entry extraction (mapping), GO annotation (annotation), and annotation augmentation (annotation). Firstly, the National Center for Biotechnology Information (NCBI) basic local alignment search tool BLAST+ (ncbi-blast-2.2.28+-win32.exe) was used to align the target protein set with the appropriate protein sequence database, and the top 10 alignment sequences satisfying E-value less than 1E-3 were retained for subsequent analysis. Secondly, the mapping process was carried out by using the Blast2GO Command Line to select the relative GO items among the target protein set and qualified items in the first step (Data version: go_201504.obo; download address: www.geneontology.org). Thirdly, in the GO annotation process, the Blast2GO Command Line takes into account the similarity of the target protein sequences and alignment sequences and source reliability of the GO item entries, and evaluates the structure of the GO graph. Subsequently, the GO item information was annotated to the target protein, which was selected in the mapping process. Fourthly, after annotation, in order to further improve the annotation efficiency, we searched the European Bioinformatics Institute (EBI) database to identify the target proteins by matching conserved motifs using InterProScan[54]. Thereafter, the motif-related functional information was annotated to the target

protein, and then ANNEX was run to further supplement the annotation information and build the connections among different kinds of GO items for improving the accuracy of annotations. In summary, the GO project described the roles of proteins in three functional categories: biological process (BP), cellular component (CC), and molecular function (MF).

The KEGG pathway annotation was used to search and compare genes in the database of KEGG GENES using the KAAS (KEGG Automatic Annotation Server) software[55], followed by the preliminary KO classification of target protein sequences. Thereafter, the information on the target proteins involved in the metabolic pathways was automatically obtained according to the KO classification. Finally, the target protein set was comprehensively analyzed using GO ontology or KEGG pathway annotation. To evaluate the protein richness of the GO ontology or KEGG pathway, the Fisher's exact test was used to compare the distribution of each GO classification or KEGG pathway in the target protein set, followed by the calculation of the significance level.

Protein clustering

In thermographic clustering analysis, the quantitative information of the target protein set was normalized to ±1 interval. Secondly, the Cluster 3.0 software (https://cluster2.software.informer.com/3.0/) was used to classify the two dimensions of the sample and protein expression simultaneously (distance algorithm: Euclidean; connection mode: Average linkage). Finally, the Java Treeview software was used to generate the hierarchical clustering thermograms.

Protein-protein interaction network

The gene symbols of the target proteins were firstly obtained from their original databases. Subsequently, the gene symbol information was used to search the database of IntAct (http://www.ebi.ac.uk/intact/main.xhtml) or STRING (http://string-db.org/) to identify the direct and indirect interactions among the target proteins according to the experimental evidence. The Cytoscape software (version 3.2.1; http://www.cytoscape.org/release_notes_3_2_1.html) was used to generate the interaction network and analyze the network.

Venn's diagrams

Venny 2.1.0 was used to find out the intersection proteins among the differentially accumulated proteins representing up- or down-regulation.

Parallel reaction monitoring (PRM) validation

To further check the levels of protein expression determined through TMT analysis, additional quantification was applied through LC-PRM MS analysis[56]. Briefly, the TMT protocol was used for peptide preparation. The stable isotope AQUA peptide was spiked in each sample and used as a standard internal reference. The tryptic peptides were loaded on stage tips of C18 for desalting prior to reversed-phase chromatography on one of the nLC-1200 easy systems (Thermo Scientific). Subsequently, 1-h liquid chromatography gradients were performed with 5–35% acetonitrile for 45 min. The Q Exactive Plus MS was applied for PRM analysis. The optimized methods for measuring the energy of collision, state of charge, and retention time of the most crucial peptides were determined by the experiments involving unique peptides with high intensities, and, therefore, each targeted protein could be handled properly. The analysis of raw data was realized via Skyline (MacCoss Lab, University of Washington)[57], wherein the intensity of signal produced by a certain peptide sequence could be quantified with respect to each sample and referenced to standards via normalization for each protein with important denatured protein samples.

Statistical analysis of data

Data were analyzed using Excel and SPSS by ANOVA followed by Tukey's significant difference test at $p \leq 0.05$. All data had three biological repeats.

Abbreviations

List of abbreviations:

Abbreviations	Full name
ASB	activity shoot bud
DSB	dormancy shoot bud
RLB	ramet leave bud
TMT	tandem mass tags
DEPs	differentially expressed proteins
SR	Ser/Arg-rich
hnRNP	heterogeneous nuclear ribonucleoprotein particle
MCM	minichromosome maintenance protein
CAD1	cinnamyl alcohol dehydrogenase 1
PAL1	phenylalanine ammonia-lyase 1
SEM	scanning electron microscope
TCA	tricarboxylic acid
BCA	bicinchoninic acid
PAGE	polyacrylamide agarose gel electrophoresis
FASP	filter-aided sample preparation
IAA	iodoacetamide
TEAB	triethylammonium bicarbonate
LC-MS/MS	liquid chromatography-tandem mass spectrometry
HCD	high-energy collisional dissociation
AGC	automatic gain control
FDR	false discovery rate
GO	Gene Ontology
NCBI	National Center for Biotechnology Information
EBI	European Bioinformatics Institute
BP	biological process
CC	cellular component
MF	molecular function
KEGG	Kyoto Encyclopedia of Genes and Genomes
PRM	Parallel reaction monitoring
PPI	Protein-Protein Interaction
PK	Pyruvate Kinase
PAL1	phenylalanine ammonia-lyase 1
SF	Splicing factor
SR	Ser/Arg-rich
ORC	origin recognition complex
PAT	polar auxin transport
LSH	LIGHT-DEPENDENT SHORT HYPOCOTYLS
LEAFY	Flower-meristem-identity gene
PI	isoelectric points

Declarations

Acknowledgement

We are thankful for the technical assistance provided by Gui Wang.

Funding

This work was supported by the National Natural Science Foundation of China (NSFC31601738), Jiangsu Modern Agricultural Industry Technology System Construction Project (JATS[2018]256).

Availability of data and materials

All data generated or analyzed in this study are included in this published article and supplementary information files.

Authors' contributions

Ling Guan designed and carried out the study, as well as wrote the manuscript. Mizhen Zhao participated in study designing and conducted the experimental work. Yaming Qian, Hongmei Yu, and Jin Xia carried out the data analysis. All authors discussed the results and reviewed the manuscript. All authors read and approved the final manuscript.

Ethics approval and consent to participate

Not applicable

Competing interests

The authors declare that they have no competing interests.

References

1. Shulaev V, Sargent DJ, Crowhurst RN, Mockler TC, Folkerts O, Delcher AL, Jaiswal P, Mockaitis K, Liston A, Mane SP *et al*: The genome of woodland strawberry (*Fragaria vesca*). *Nature genetics* 2011, 43(2):109-116.

2. Isobe S.N. SK, Nagano S., Hirakawa H. : Current Status of Octoploid Strawberry (Fragaria×ananassa) Genome Study. . *Compendium of Plant Genomes Springer, Cham* 2018.

3. D. S: The economic importance of strawberry crops. In: Hytönen T., Graham J., Harrison R. (eds) The genomes of rosaceous berries and their wild relatives. *Compendium of Plant Genomes Springer, Cham* 2018.

4. Darrow GM: The strawberry: History, Breeding and Physiology. . *Holt, Rinehart and Winston, New York, USA* 1966.

5. Costes E, Crespel, L., Denoyes, B., Morel, P., Demene, M. N., Lauri, P. E., & Wenden, B.: Bud structure, position and fate generate various branching patterns along shoots of closely related Rosaceae species: a review. *Frontiers in plant science,* 2014 5(666).

6. Tenreira T, Lange MJP, Lange T, Bres C, Labadie M, Monfort A, Hernould M, Rothan C, Denoyes B: A Specific gibberellin 20-Oxidase dictates the flowering-runnering decision in diploid strawberry. *The Plant Cell* 2017, 29(9):2168.

7. Alpert P, Mooney HA: Resource sharing among ramets in the clonal herb, Fragaria chiloensis. *Oecologia* 1986, 70(2):227-233.

8. Atkinson CJ, Else MA: Hydraulic conductivity and PAT determine hierarchical resource partitioning and ramet development along Fragaria stolons. *Journal of Experimental Botany* 2012, 63(14): 5093-5104.

9. Caruana JC, Sittmann JW, Wang W, Liu Z: Suppressor of runnerless encodes a DELLA protein that controls runner formation for asexual reproduction in strawberry. *Molecular Plant* 2018, 11(1):230-233.

10. Fang X, Ma H, Lu D, Yu H, Lai W, Ruan S: Comparative proteomics analysis of proteins expressed in the I-1 and I-2 internodes of strawberry stolons. *Proteome Science* 2011, 9(1):26.

11. Liu S, Gao J, Chen Z, Qiao X, Huang H, Cui B, Zhu Q, Dai Z, Wu H, Pan Y *et al*: Comparative proteomics reveals the physiological differences between winter tender shoots and spring tender shoots of a novel tea (*Camellia sinensis* L.) cultivar evergrowing in winter. *BMC Plant Biology* 2017, 17(1):206.

12. Li LQ, Zou X, Deng MS, Peng J, Huang XL, Lu X, Fang CC, Wang XY: Comparative morphology, transcription, and proteomics study revealing the key molecular mechanism of camphor on the potato tuber sprouting effect. *Int J Mol Sci* 2017, 18(11).

13. Du H, Shi Y, Li D, Fan W, Wang Y, Wang G, Wang C: Proteomics reveals key proteins participating in growth difference between fall dormant and non-dormant alfalfa in terminal buds. *Journal of Proteomics* 2018, 173:126-138.

14. O'Brien EJ, Palsson BO: Computing the functional proteome: recent progress and future prospects for genome-scale models. *Current Opinion in Biotechnology* 2015, 34:125-134.

15. Thompson A, Schäfer J, Kuhn K, Kienle S, Schwarz J, Schmidt G, Neumann T, Hamon C: Tandem Mass Tags: A Novel Quantification Strategy for Comparative Analysis of Complex Protein Mixtures by MS/MS. *Analytical Chemistry* 2003, 75(8):1895-1904.

16. Savini G, Giorgi V, Scarano E, Neri D: Strawberry plant relationship through the stolon. *Physiologia Plantarum* 2008, 134(3):421-429.

17. Shimizu-Sato S, Mori H: Control of outgrowth and dormancy in axillary buds. *Plant Physiology* 2001, 127(4):1405.

18. Barbier FF, Dun EA, Beveridge CA: Apical dominance. *Current Biology* 2017, 27(17):R864-R865.

19. Chen X, Xia X, Guo X, Zhou Y, Shi K, Zhou J, Yu J: Apoplastic H_2O_2 plays a critical role in axillary bud outgrowth by altering auxin and cytokinin homeostasis in tomato plants. *New Phytologist* 2016, 211(4):1266-1278.

20. Zhao C, Zhao S, Hou L, Xia H, Wang J, Li C, Li A, Li T, Zhang X, Wang X: Proteomics analysis reveals differentially activated pathways that operate in peanut gynophores at different developmental stages. *BMC Plant Biology* 2015, 15(1):188.

21. Fan W, Ge G, Liu Y, Wang W, Liu L, Jia Y: Proteomics integrated with metabolomics: analysis of the internal causes of nutrient changes in alfalfa at different growth stages. *BMC Plant Biology* 2018, 18(1):78.

22. Lei C, Fan S, Li K, Meng Y, Mao J, Han M, Zhao C, Bao L, Zhang D: iTRAQ-based proteomic analysis reveals potential regulation networks of IBA-induced adventitious root formation in apple. *Int J Mol Sci* 2018, 19(3).

23. Li M, Wu X, Guo X, Bao P, Ding X, Chu M, Liang C, Yan P: Comparative iTRAQ proteomics revealed proteins associated with horn development in yak. *Proteome Science* 2018, 16(1):14.

24. Uhlén M, Fagerberg L, Hallström BM, Lindskog C, Oksvold P, Mardinoglu A, Sivertsson Å, Kampf C, Sjöstedt E, Asplund A *et al*: Tissue-based map of the human proteome. *Science* 2015, 347(6220):1260419.

25. Yves Meyer MM-M, Peter Schürmann, Jean-Pierre Jacquot: Protein-protein interactions in plant biology. *In Annual Plant Reviews online, J A Roberts (Ed)* 2002, 7.

26. Smits AH, Vermeulen M: Characterizing Protein–protein interactions using mass spectrometry: challenges and opportunities. *Trends in Biotechnology* 2016, 34(10):825-834.

27. Stelzl U, Worm U, Lalowski M, Haenig C, Brembeck FH, Goehler H, Stroedicke M, Zenkner M, Schoenherr A, Koeppen S *et al*: A human protein-protein interaction network: a resource for annotating the proteome. *Cell* 2005, 122(6):957-968.

28. Kumar C, Mann M: Bioinformatics analysis of mass spectrometry-based proteomics data sets. *FEBS Letters* 2009, 583(11):1703-1712.

29. Lorković ZJ: Role of plant RNA-binding proteins in development, stress response and genome organization. *Trends in Plant Science* 2009, 14(4):229-236.

30. Matteo S, Vittoria B, Emile J M C, Maarten K, Wim J J S: The conserved splicing factor *SUA* controls alternative splicing of the developmental regulator *ABI3* in Arabidopsis. *The Plant Cell* 2010, 22(6):1936-1946.

31. Agafonov DE, Deckert J, Wolf E, Odenwälder P, Bessonov S, Will CL, Urlaub H, Lührmann R: Semiquantitative proteomic analysis of the human spliceosome via a novel two-dimensional gel electrophoresis method. *Molecular and Cellular Biology* 2011, 31(13):2667.

32. Halaly T, Pang X, Batikoff T, Crane O, Keren A, Venkateswari J, Ogrodovitch A, Sadka A, Lavee S, Or E: Similar mechanisms might be triggered by alternative external stimuli that induce dormancy release in grape buds. *Planta* 2008, 228(1):79-88.

33. Wang SY, Jiao HJ, Faust M: Changes in metabolic enzyme activities during thidiazuron-induced lateral budbreak of apple. *HortScience* 1991, 26(2):171-173.

34. Bonhomme M, Rageau R, Gendraud M: Influence of temperature on the dynamics of ATP, ADP and non-adenylic triphosphate nucleotides in vegetative and floral peach buds during dormancy. *Tree Physiology* 2000, 20(9):615.

35. Mimura S, Kubota Y, Takisawa H: MCM interference during licensing of DNA replication in Xenopus egg extracts-possible role of a C-terminal region of MCM3. *Cell Cycle* 2018, 17(4):492-505.

36. Liang Z, Li W, Liu J, Li J, He F, Jiang Y, Yang L, Li P, Wang B, Wang Y *et al*: Simvastatin suppresses the DNA replication licensing factor *MCM7* and inhibits the growth of tamoxifen-resistant breast cancer cells. *Scientific Reports* 2017, 7:41776.

37. Chevalier C: Cell Cycle Control and Fruit Development; 2007.

38. Cary AJ, Che P, Howell SH: Developmental events and shoot apical meristem gene expression patterns during shoot development in *Arabidopsis thaliana*. *The Plant Journal* 2002, 32(6):867-877.

39. Motte H, Galuszka P, Spíchal L, Tarkowski P, Plíhal O, Šmehilová M, Jaworek P, Vereecke D, Werbrouck S, Geelen D: Phenyl-adenine, identified in a LIGHT-DEPENDENT SHORT HYPOCOTYLS4- assisted chemical screen, is a potent compound for shoot regeneration through the inhibition of CYTOKININ OXIDASE/DEHYDROGENASE activity. *Plant Physiology* 2013, 161(3):1229.

40. Pernisová M, Klíma P, Horák J, Válková M, Malbeck J, Souček P, Reichman P, Hoyerová K, Dubová J, Friml J *et al*: Cytokinins modulate auxin-induced organogenesis in plants via regulation of the auxin efflux. *Proceedings of the National Academy of Sciences* 2009, 106(9):3609.

41. Weigel D, Nilsson O: A developmental switch sufficient for flower initiation in diverse plants. *Nature* 1995, 377:495.

42. Li G, Zhao B, Dong S, Zhang J, Liu P, Vyn TJ: Interactive effects of water and controlled release urea on nitrogen metabolism, accumulation, translocation, and yield in summer maize. *The Science of Nature* 2017, 104(9):72.

43. Stewart GR, Shatilov VR, Turnbull MH, Robinson SA, Goodall R: Evidence that glutamate dehydrogenase plays a role in the oxidative deamination of glutamate in seedlings of *Zea mays*. *Functional Plant Biology* 1995, 22(5):805-809.

44. Helling RB: Pathway choice in glutamate synthesis in Escherichia coli. *Journal of Bacteriology* 1998, 180(17):4571.

45. Singh RP, Srivastava HS: Increase in glutamate synthase (NADH) activity in maize seedlings in response to nitrate and ammonium nitrogen. *Physiologia Plantarum* 1986, 66(3):413-416.

46. Ferrer JL, Austin MB, Stewart C, Noel JP: Structure and function of enzymes involved in the biosynthesis of phenylpropanoids. *Plant Physiology and Biochemistry* 2008, 46(3):356-370.

47. Boerjan W, Ralph J, Baucher M: Lignin Biosynthesis. *Annual Review of Plant Biology* 2003, 54(1):519-546.

48. Feng H, Xu L, Wang Y, Tang M, Zhu X, Zhang W, Sun X, Nie S, Muleke EMm, Liu L: Identification of critical genes associated with lignin biosynthesis in radish (*Raphanus sativus* L.) by de novo transcriptome sequencing. *Molecular Genetics and Genomics* 2017, 292(5):1151-1163.

49. Van Acker R, Déjardin A, Desmet S, Hoengenaert L, Vanholme R, Morreel K, Laurans F, Kim H, Santoro N, Foster C *et al*: Different routes for conifer- and sinapaldehyde and higher saccharification upon deficiency in the dehydrogenase CAD1. *Plant Physiology* 2017, 175(3):1018.

50. Jorrín Novo JV: Plant Proteomics: Methods and Protocols. By Hervé Thiellement, Michel Zivy, Catherine Damerval and Valérie Mechin (Eds.). *Biotechnology Journal* 2007, 2(5):642-642.

51. Wisniewski JR, Zougman A, Nagaraj N, Mann M: Universal sample preparation method for proteome analysis. *Nature methods* 2009, 6(5):359-362.

52. Isobe SN, Hirakawa H, Sato S, Maeda F, Ishikawa M, Mori T, Yamamoto Y, Shirasawa K, Kimura M, Fukami M *et al*: Construction of an integrated high density simple sequence repeat linkage map in cultivated strawberry (*Fragaria* x *ananassa*) and its applicability. *DNA Res* 2013, 20(1):79-92.

53. Götz S, García-Gómez JM, Terol J, Williams TD, Nagaraj SH, Nueda MJ, Robles M, Talón M, Dopazo J, Conesa A: High-throughput functional annotation and data mining with the Blast2GO suite. *Nucleic Acids Research* 2008, 36(10):3420-3435.

54. Quevillon E, Silventoinen V, Pillai S, Harte N, Mulder N, Apweiler R, Lopez R: InterProScan: protein domains identifier. *Nucleic Acids Research* 2005, 33(suppl_2):W116-W120.

55. Moriya Y, Itoh M, Okuda S, Yoshizawa AC, Kanehisa M: KAAS: an automatic genome annotation and pathway reconstruction server. *Nucleic Acids Research* 2007, 35(suppl_2):W182-W185.

56. Peterson AC, Russell JD, Bailey DJ, Westphall MS, Coon JJ: Parallel reaction monitoring for high resolution and high mass accuracy quantitative, targeted proteomics. *Molecular & Cellular Proteomics* 2012:mcp.O112.020131.

57. MacLean B, Tomazela DM, Shulman N, Chambers M, Finney GL, Frewen B, Kern R, Tabb DL, Liebler DC, MacCoss MJ: Skyline: an open source document editor for creating and analyzing targeted proteomics experiments. *Bioinformatics* 2010, 26(7):966-968.

Tables

Table 1. *Top 10 of up- and down-regulated differentially expressed proteins between groups*

Groups	No.	Protein ID	Description	Coverage	Fold change	P-value
ASB/DSB	up-1	XP_004304418.1	Fasciclin-like arabinogalactan protein 12	20.73	6.23	0.00186255
	up-2	FANhyb_rscf00000173.1.g00014.1	hypothetical protein CARUB_v10021660mg	22.06	5.29	0.02442
	up-3	FANhyb_rscf00000386.1.g00003.1	fasciclin-like arabinogalactan protein 12	20.73	4.78	1.3548E-07
	up-4	XP_011462288.1	glycine-rich cell wall structural protein	50.36	4.64	0.015453
	up-5	XP_004299681.1	blue copper protein-like	14.21	4.52	0.004586
	up-6	FANhyb_rscf00004026.1.g00001.1	glucuronoxylan 4-O-methyltransferase 3-like	7.36	3.80	0.00520136
	up-7	FANhyb_icon00011962_a.1.g00001.1	fructokinase-5	38.28	3.61	0.00072744
	up-8	XP_011458504.1	anthocyanidin 3-O-glucosyltransferase 7-like	19.91	3.53	0.00100593
	up-9	FANhyb_rscf00000027.1.g00021.1	zinc finger protein	2.58	3.47	0.00693375
	up-10	FANhyb_rscf00000295.1.g00005.1	histone H2A.1	37.84	3.43	0.00117360739903088
	down-1	XP_004307317.1	cucumisin-like	7.83	0.34	0.01617526
	down-2	XP_004307401.1	serine carboxypeptidase-like 27	11.79	0.35	0.01705444
	down-3	FANhyb_rscf00000020.1.g00007.1	pectinesterase	4.17	0.37	0.03259767
	down-4	XP_004297134.2	ornithine decarboxylase-like	4.66	0.38	0.00237870
	down-5	FANhyb_rscf00000011.1.g00007.1	36.4 kDa proline-rich protein	9.32	0.38	0.00620498
	down-6	FANhyb_icon00014184_a.1.g00001.1	putative laccase-9	2.76	0.41	0.01597461
	down-7	XP_004303137.1	ribulose bisphosphate carboxylase small chain, chloroplastic-like	31.87	0.42	0.01480696
	down-8	FANhyb_rscf00001104.1.g00003.1	aquaporin TIP2-1	7.26	0.43	0.00599268
	down-9	FANhyb_icon00031506_a.1.g00001.1	putative 4-hydroxy-4-methyl-2-oxoglutarate aldolase 2	47.83	0.45	0.00430290
	down-10	XP_004293363.1	fruit protein pKIWI501-like	50.00	0.45	0.02295962
RLB/DSB	up-1	XP_004303183.1	protein LIGHT-	13.88	3.24	0.01882948

		DEPENDENT SHORT HYPOCOTYLS 10-like			
up-2	FANhyb_rscf00005475.1.g00002.1	pentatricopeptide repeat-containing protein At4g38150-like	10.04	2.29	0.013968033783
up-3	XP_004307632.1	flocculation protein FLO11 isoform X3	2.47	1.76	0.00227661
up-4	FANhyb_rscf00000173.1.g00014.1	hypothetical protein CARUB_v10021660mg	22.06	1.76	0.00017183
up-5	FANhyb_icon00004730_a.1.g00001.1	squamosa promoter-binding-like protein 9	7.09	1.69	0.00267638
up-6	FANhyb_rscf00000264.1.g00010.1	uncharacterized protein LOC101290827	12.68	1.61	0.03225374
up-7	XP_011462288.1	glycine-rich cell wall structural protein	50.36	1.58	0.00426962
up-8	XP_004299681.1	blue copper protein-like	14.21	1.58	0.00418736
up-9	XP_004310149.1	mediator-associated protein 2	10.27	1.57	0.04857720
up-10	FANhyb_rscf00005241.1.g00001.1	zinc-finger homeodomain protein 6	16.35	1.56	0.02325629
down-1	XP_004307317.1	cucumisin-like	7.83	0.41	0.02484890
down-2	XP_004297134.2	ornithine decarboxylase-like	4.66	0.41	0.00581982
down-3	XP_004307401.1	serine carboxypeptidase-like 27	11.79	0.41	0.02026585
down-4	FANhyb_rscf00001190.1.g00001.1	telomere repeat-binding factor 1-like	9.04	0.50	0.00752576
down-5	FANhyb_rscf00000011.1.g00007.1	36.4 kDa proline-rich protein	9.32	0.51	0.01674637
down-6	FANhyb_rscf00000159.1.g00006.1	glyceraldehyde-3-phosphate dehydrogenase B, chloroplastic	14.16	0.54	0.01030551
down-7	FANhyb_rscf00005433.1.g00001.1	fasciclin-like arabinogalactan protein 13	8.54	0.55	0.00275099
down-8	XP_004303137.1	ribulose bisphosphate carboxylase small chain, chloroplastic-like	31.87	0.56	0.03678190
down-9	FANhyb_icon00037348_a.1.g00001.1	ribulose bisphosphate carboxylase small chain,	54.00	0.56	0.03512944

			chloroplastic-like			
	down-10	XP_004297630.1	carbonic anhydrase 2 isoform X2	19.37	0.57	0.00032382
RLB/ASB	up-1	FANhyb_rscf00000329.1.g00005.1	1-aminocyclopropane-1-carboxylate oxidase 1-like	16.07	2.16	0.00162178
	up-2	FANhyb_rscf00001394.1.g00002.1	glutamate dehydrogenase 1	20.87	2.05	0.04362181
	up-3	FANhyb_icon00031506_a.1.g00001.1	putative 4-hydroxy-4-methyl-2-oxoglutarate aldolase 2	47.83	2.05	0.00751062
	up-4	XP_004293441.1	major latex allergen Hev b 5-like	68.04	2.04	0.00379106
	up-5	XP_004293363.1	fruit protein pKIWI501-like	50	2.00	0.00846049
	up-6	FANhyb_rscf00001104.1.g00003.1	aquaporin TIP2-1	7.26	1.98	0.00734669
	up-7	FANhyb_rscf00000704.1.g00001.1	putative formamidase C869.04 isoform X1	3.69	1.98	0.01632577
	up-8	FANhyb_rscf00005475.1.g00002.1	pentatricopeptide repeat-containing protein At4g38150-like	10.04	1.89	0.02607894
	up-9	FANhyb_rscf00000980.1.g00003.1	glutathione S-transferase F13-like	43.45	1.81	0.00588200
	up-10	XP_004291285.2	probable sarcosine oxidase	8.69	1.80	0.00202212
	down-1	XP_004304418.1	fasciclin-like arabinogalactan protein 12	20.73	0.23	0.00070797
	down-2	FANhyb_rscf00000386.1.g00003.1	fasciclin-like arabinogalactan protein 12	20.73	0.25	0.00001714
	down-3	FANhyb_rscf00004026.1.g00001.1	glucuronoxylan 4-O-methyltransferase 3-like	7.36	0.29	0.00706772
	down-4	XP_011457444.1	F-box protein SKIP14	2.38	0.30	0.00827485
	down-5	FANhyb_icon00004976_a.1.g00001.1	cytochrome P450 84A1	28.68	0.31	7.5325E-07
	down-6	XP_004294339.1	probable galacturonosyltransferase 12	3.00	0.31	0.01158193
	down-7	FANhyb_rscf00000173.1.g00014.1	|hypothetical protein CARUB_v10021660mg	22.06	0.33	0.04426256
	down-8	XP_011462288.1	glycine-rich cell wall	50.36	0.34	0.02679911

		structural protein			
down-9	XP_004299681.1	blue copper protein-like	14.21	0.35	0.03378082
down-10	FANhyb_rscf00002637.1.g00001.1	L-type lectin-domain-containing receptor kinase IX.1-like	2.04	0.35	0.03378082

Table 2 *DEPs with high connectivity degree in PPI analysis between groups*

Group	Protein accession	Degree	Description	Unique peptide	Fold Change
ASB/DSB	XP_004304484.1	42	splicing factor 3A subunit 2 isoform X1	5	1.29
	FANhyb_rscf00000157.1.g00010.1	37	60S ribosomal protein L7a-2	6	1.24
	FANhyb_rscf00000522.1.g00007.1	37	small nuclear ribonucleoprotein-associated protein B & apos	3	1.31
	XP_004290666.1	36	small nuclear ribonucleoprotein Sm D1-like	4	1.28
	XP_004303828.1	35	60S ribosomal protein L7-2	2	1.53
	XP_004287907.1	34	U1 small nuclear ribonucleoprotein 70 kDa	10	1.36
	XP_004308170.1	33	40S ribosomal protein S20-2	6	1.28
	XP_004299660.1	33	40S ribosomal protein S6	8	1.25
	FANhyb_rscf00005750.1.g00001.1	33	30S ribosomal protein S17, chloroplastic-like	2	1.27
	XP_004307020.1	33	pyruvate kinase, cytosolic isozyme-like	16	0.83
	XP_004304484.1	42	splicing factor 3A subunit 2 isoform X1	5	1.29
	XP_004297699.1	33	pyruvate kinase, cytosolic isozyme-like	18	0.82
	FANhyb_icon14422311_s.1.g00001.1	32	60S ribosomal protein L27a-3	2	1.28
	XP_004296676.1	32	60S ribosomal protein L27a-3	2	1.24
	XP_004306930.1	32	40S ribosomal protein S13	1	1.62
	FANhyb_rscf00000738.1.g00007.1	32	serine/arginine-rich splicing factor RS31-like isoform X1	7	1.50
	XP_004306844.1	32	serine/arginine-rich splicing factor RS41-like isoform X1	5	1.50
	XP_011470401.1	32	serine/arginine-rich splicing factor RS41 isoform X1	5	1.29
	XP_004300041.1	31	uncharacterized RNA-binding protein C1827.05c	3	1.26
	XP_004299114.1	31	SART-1 family protein DOT2	12	1.26
	XP_004297699.1	33	pyruvate kinase, cytosolic isozyme-like	18	0.82
RLB/DSB	FANhyb_icon00002169_a.1.g00001.1	19	LOW QUALITY PROTEIN: replication factor C subunit 1	1	1.37
	XP_011458268.1	12	DNA replication licensing factor MCM4	18	1.22
	XP_004299199.1	12	protein LIGHT-DEPENDENT SHORT HYPOCOTYLS 10-like	1	3.24
	FANhyb_icon00004233_a.1.g00001.1	12	structural maintenance of chromosomes protein 2-1-like	1	1.46
	XP_011460181.1	11	DNA replication licensing factor MCM3	2	1.26
	XP_004300454.1	11	DNA replication licensing factor MCM7	18	1.27
RLB/ASB	FANhyb_rscf00000086.1.g00005.1	16	glutamate synthase 1 [NADH], chloroplastic isoform X1	20	0.74
	XP_004299600.1	15	acetyl-CoA carboxylase 1-like isoform X1	29	0.65
	XP_004297699.1	14	pyruvate kinase, cytosolic isozyme-like	14	1.23
	FANhyb_icon00042639_a.1.g00001.1	12	hypothetical protein B456_008G262000	1	0.75
	FANhyb_rscf00005750.1.g00001.1	12	30S ribosomal protein S17, chloroplastic-like	2	0.77
	XP_004308170.1	12	40S ribosomal protein S20-2	6	0.81
	FANhyb_rscf00001394.1.g00002.1	12	glutamate dehydrogenase 1	5	2.05
	XP_004287377.1	12	probable histone H2A variant 3	2	0.54
	XP_004309949.1	12	4-coumarate-CoA ligase 2-like	4	0.50
	FANhyb_rscf00001010.1.g00003.1	11	40S ribosomal protein S24-1-like	1	0.80
	FANhyb_rscf00000697.1.g00007.1	11	40S ribosomal protein S24-1	1	0.69

Figures

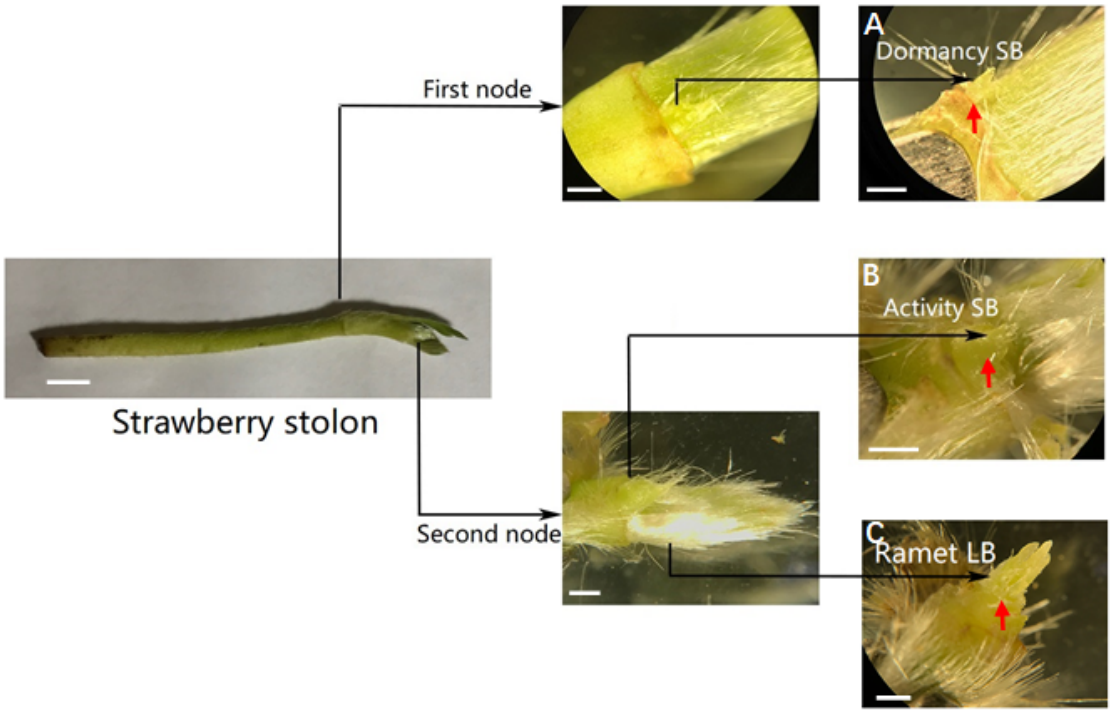

Figure 1

Three bud physiological statuses in the first node [A, dormancy shoot bud (DSB)] and the second node [B, activity shoot bud (ASB) and C, ramet leave bud (RLB)] of strawberry stolon. The scale bar in the figure showing whole strawberry stolon is 1 cm, and in the other figures is 1 mm.

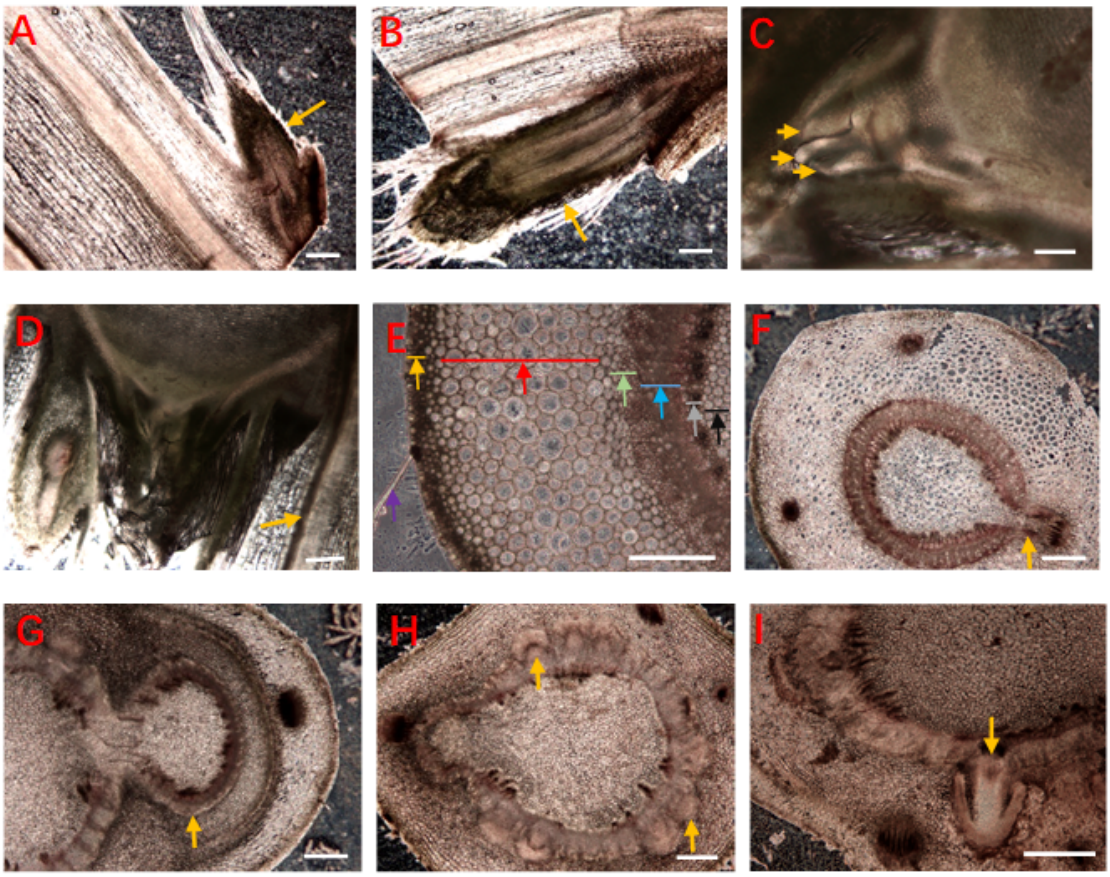

Figure 2

Slice observation of strawberry stolon. (A) Growth arrest in the first node and its stepping into dormancy, (B) Continuous development as a new stolon branch upon dormancy release. (C) Arrows indicate the trifoliolate ramet leave buds in the second node. (D) Vascular bundles (arrow) of the new developing stolon in the second node connected to the primary stolon. (E) The tissues from the outside to the inside of the stolon are epidermal hair (purple) and epidermis (orange), thick cortex (red), cambium (green; composed a large number of parenchymatous cells), phloem (blue), xylem (grey), and pith (black). (F–G) vascular of the lateral buds on the first (F, orange arrow) and second nodes (G, orange arrow) of the strawberry stolon were connected inward with the primary stolon vascular. (H-I) adventitious root primordia, which originated from the cambium. The scale bar is 0.5 mm in figures A-B and F-I, 1 mm in figure C-D, and 0.3 mm in figure E.

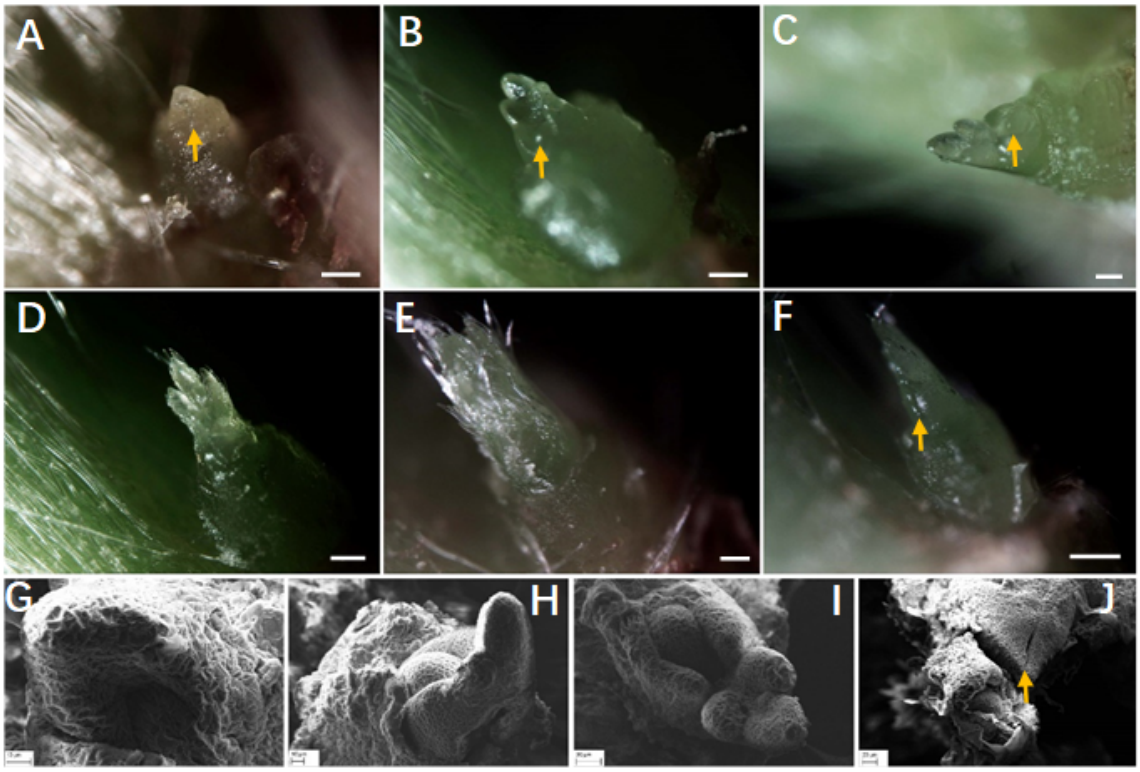

Figure 3

Dormancy shoot bud (DSB) developmental phases in the first node. (A–C) Three typical developmental phases of DSB (arrow) at the early stage of primary stolon elongation. (D–E) DSB covered by a young trifoliolate leaf bract. (F) closed bract with a DSB inside. (G–J) scanning electron microscope (SEM) photomicrographs of DSB in A–C and F. The scale bar is 10 μm in A, 25 μm in B, 50 μm in C, 100 μm in D–E, 150 μm in F, 10 μm in G–H, and 20 μm in I–J.

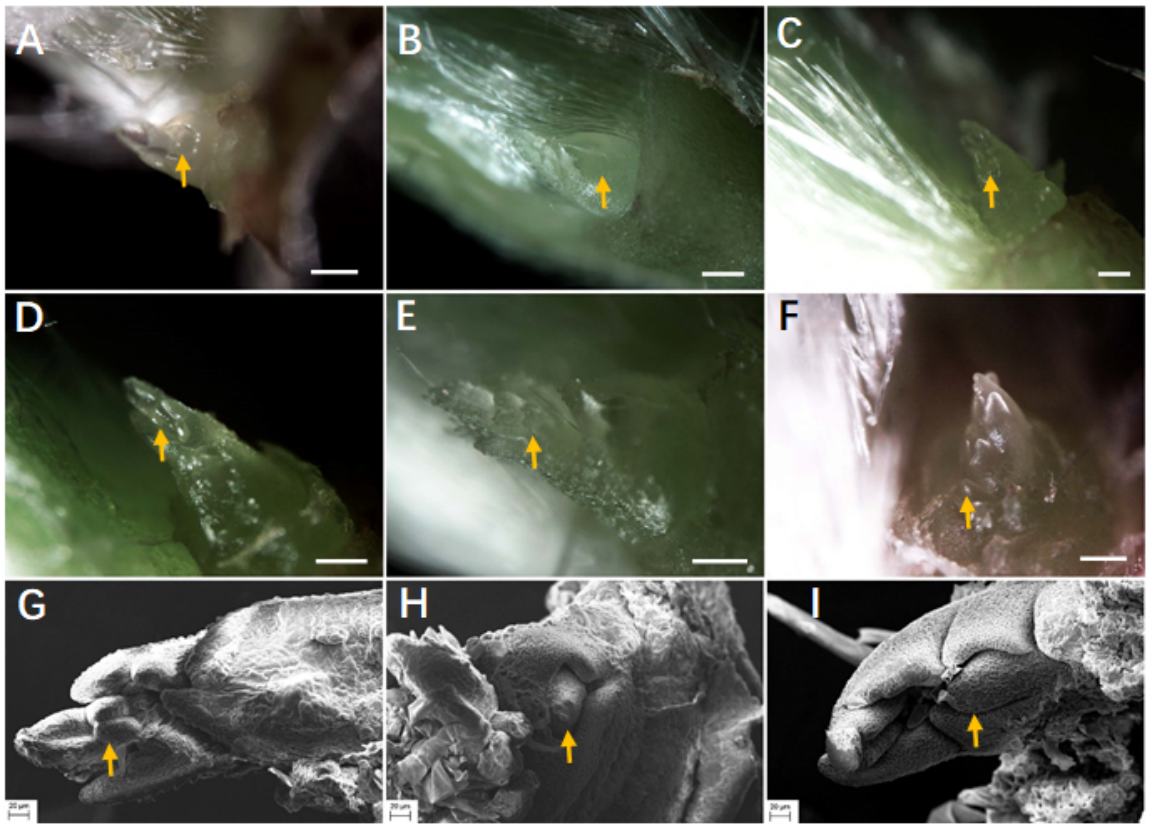

Figure 4

Activity shoot bud (ASB) development in the second node. (A–B) ASB primordium located at the center of the developing and matured bract. (C–E) ASB apex development when the matured bract was peeled off. (F) ASB structure when the young apex of ASB was peeled off again and a new growth point (arrow). (G–I) are the respective SEM observations for D–F; in these figures, we know the trifoliolate apex exhibited a high developmental activity. The scale bar is 50 μm in A-D, 100 μm in E–F, and 20 μm in G–I.

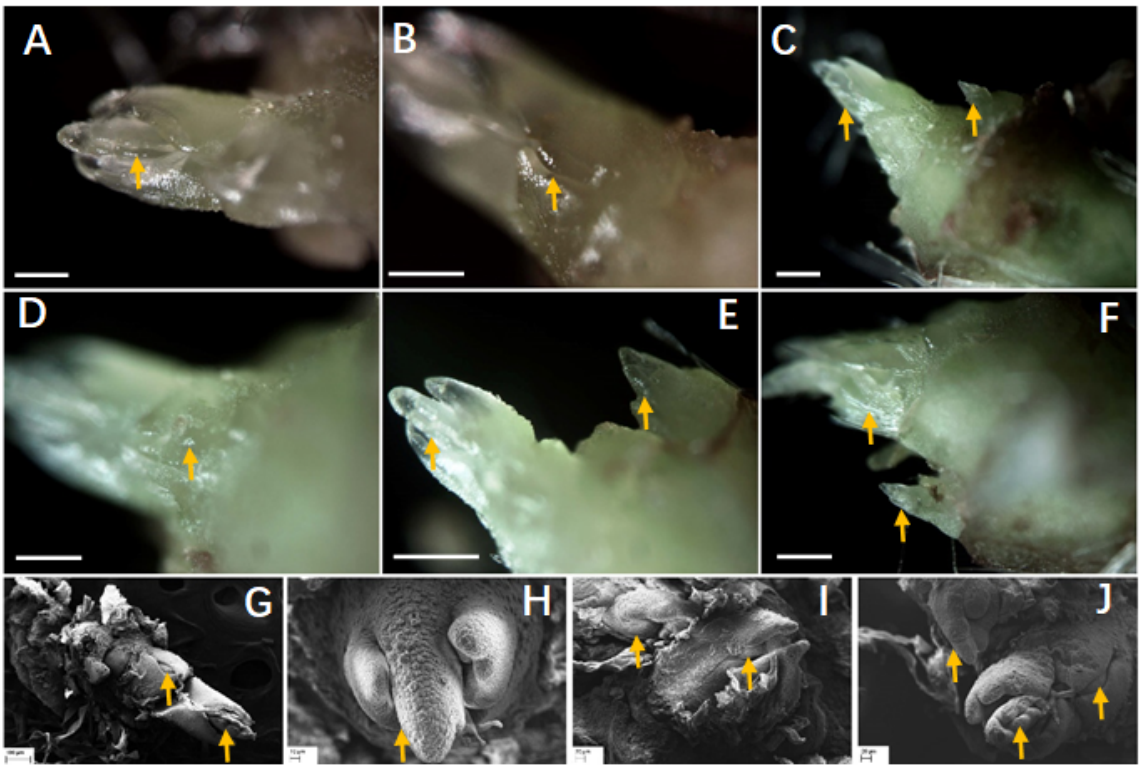

Figure 5

Ramet leave bud (RLB) development in the second node of a strawberry stolon. (A) Pure trifoliolate leave enclosed in the bract. (B) Newly formed bract, with a new primordium of trifoliolate leaves inside. (C–E) show the development of ramet leave buds and laterally located newly formed stolon buds. (F) young trifoliolate cluster and laterally located new stolon in the second node. (G and H) detailed exhibition of ramet leave buds cluster and the bird's eye perspective of a single developing leaf bud, respectively. (I–J) show the development of laterally located newly formed stolon buds with the growth of apical ramet buds. The scale bar is 150 μm in A–B and D–E, 300 μm in C and F, 100 μm in G, 10 μm in H, and 20 μm in I–J.

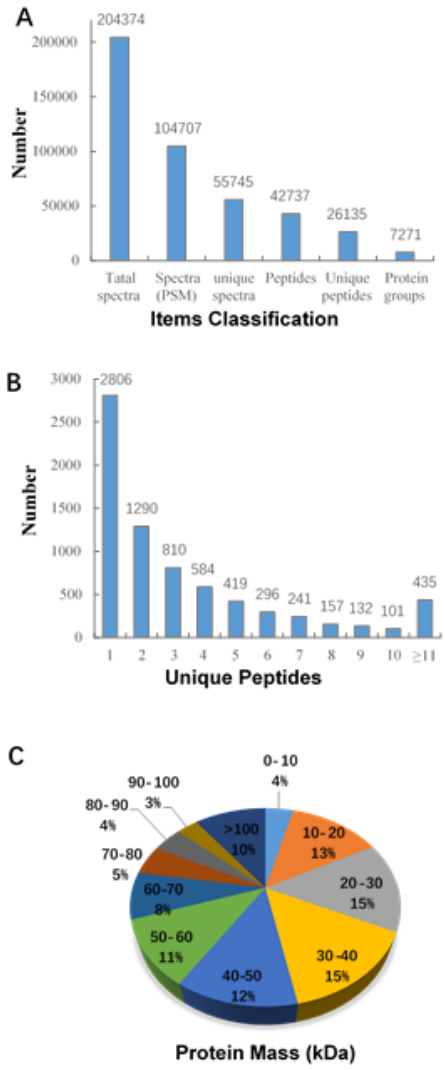

Figure 6

Results of the tandem mass tags (TMT)–based liquid chromatography-tandem mass spectrometry (LC-MS/MS) identification of the stolon buds of the Ning Yu variety of strawberry. (A) The classification of the items used in identifying proteins; (B) Number of unique peptides that were matched to each identified protein; (C) Distribution of the average molecular mass of identified proteins.

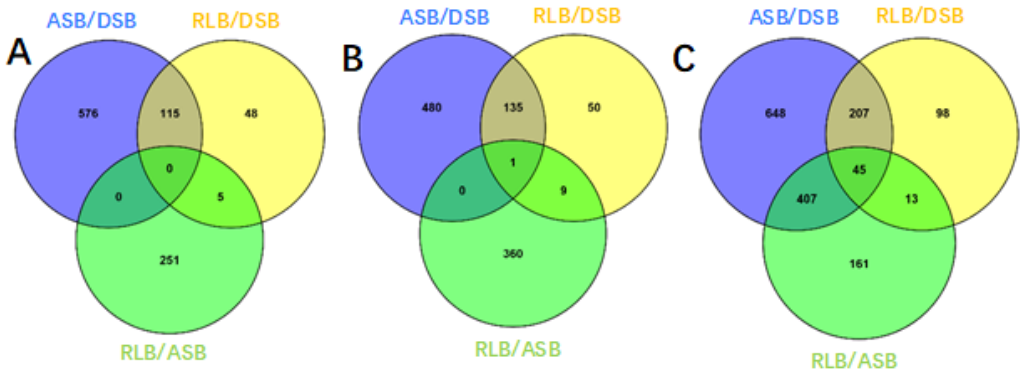

Figure 7

Venn diagram of DEPs that have Co-up (A) and co-down (B), as well as total co-up plus co-down (C) expressions from each experimental group comparison

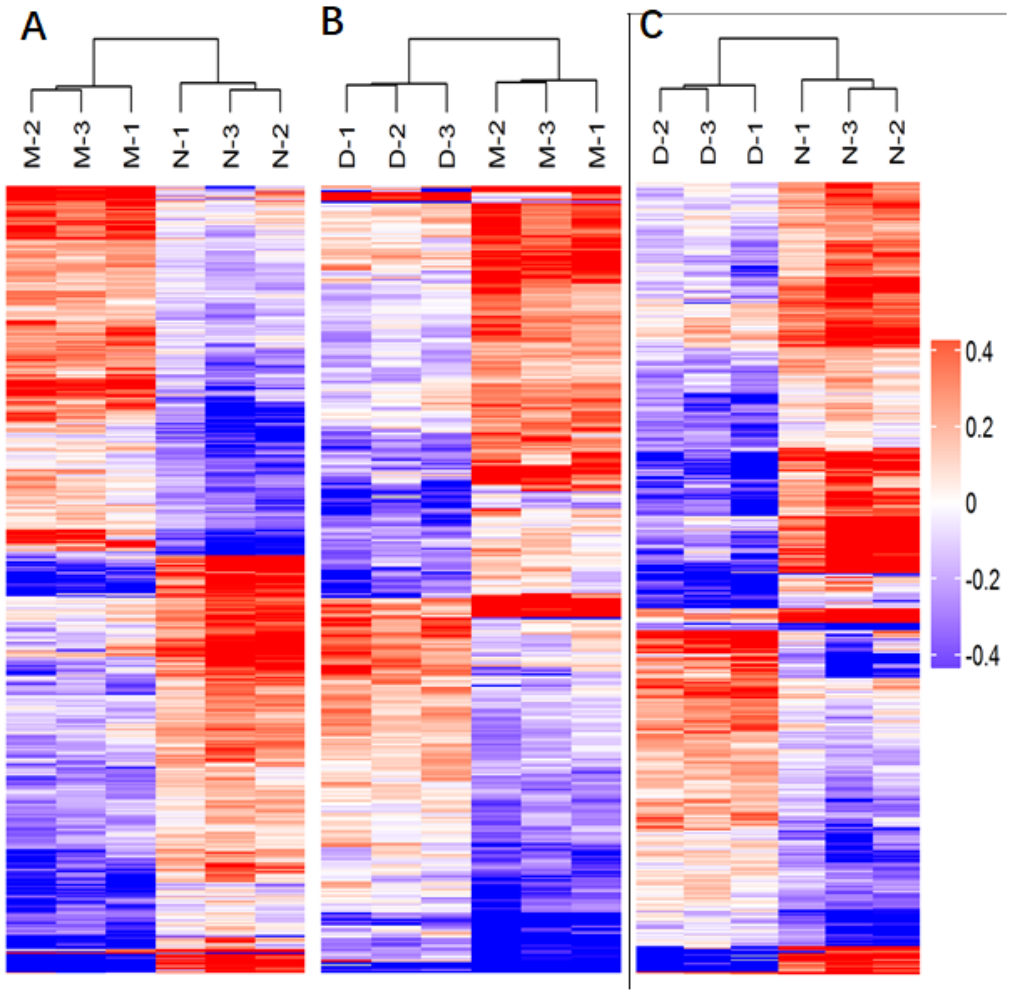

Figure 8

Cluster analysis of differentially expressed proteins. Through horizontal comparison, samples could be classified into three categories, suggesting that the selected DEPs could effectively distinguish between samples. A vertical comparison indicated that proteins could be classified into two categories with opposite directional variation, demonstrating the rationality of the selected DEPs. M, N, and D represent the DSB, ASB, and RLB groups, respectively. (A) is DSB/ASB, (B) is RLB/DSB, and (C) is RLB/ASB.

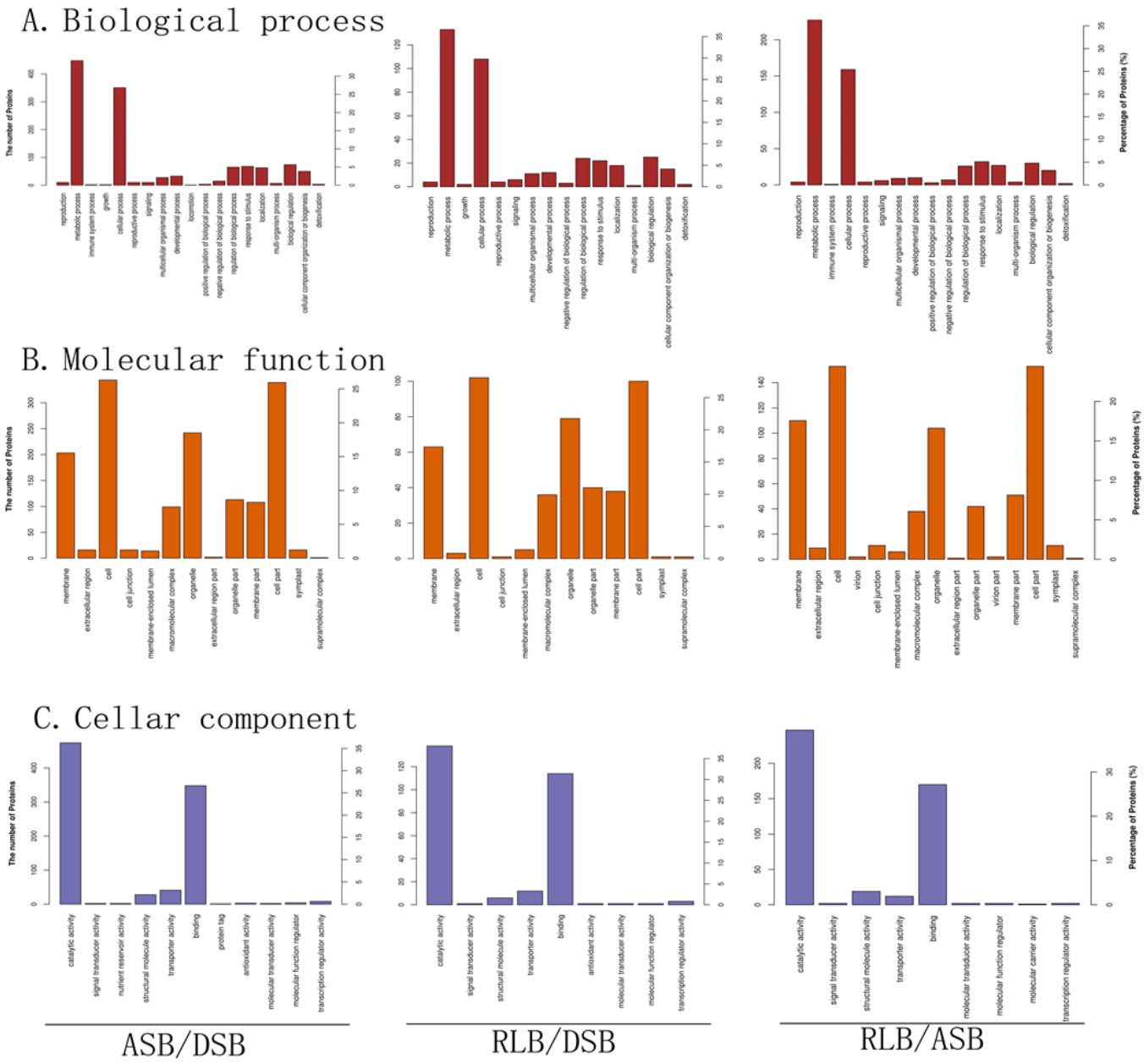

Figure 9

Gene ontology annotation of differentially expressed proteins (DEPs) among groups. The X-axis represents the Gene Ontology functional classification. The main Y-axis represents the number of DEPs, and the secondary Y-axis represents the classified DEP ratio in respective group's total DEPs (ASB/DSB, RLB/DSB and RLB/ASB). A, Biological process. B, Molecular function. C, Cellular component.

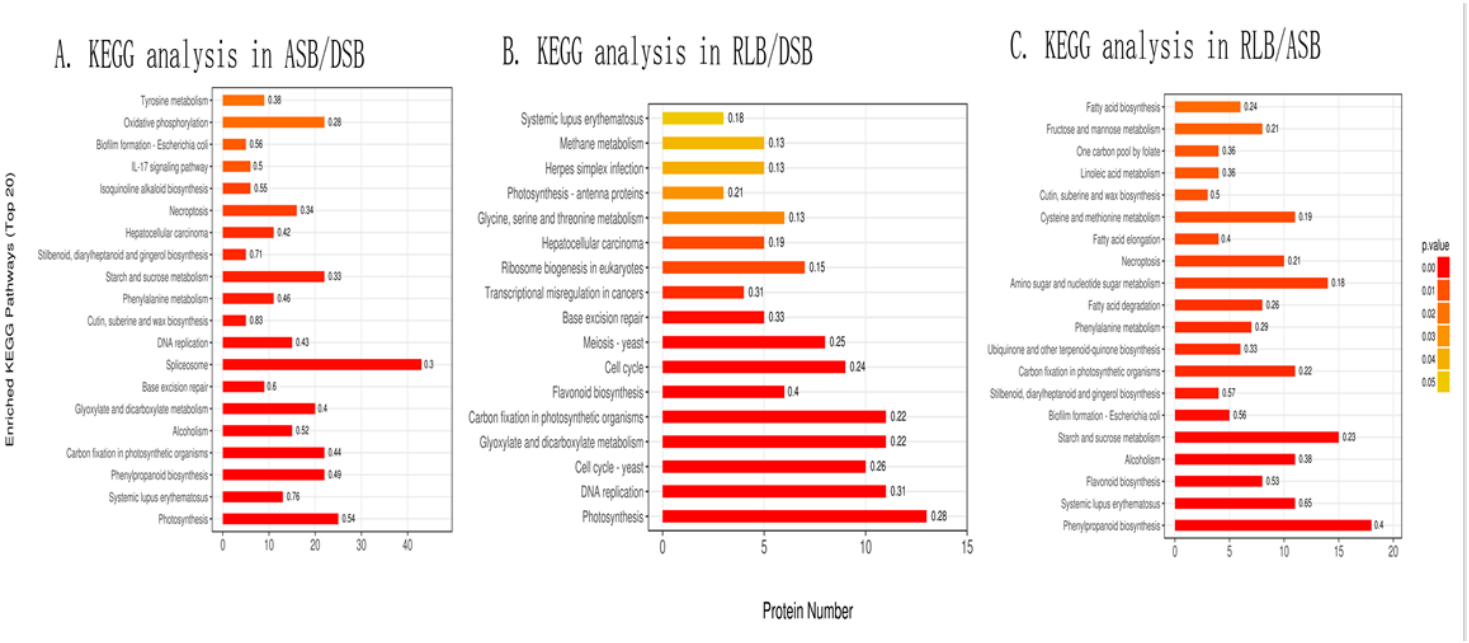

Figure 10

KEGG Pathway Analysis between different groups of ASB/DSB (A), RLB/DSB (B), and RLB/ASB (C).

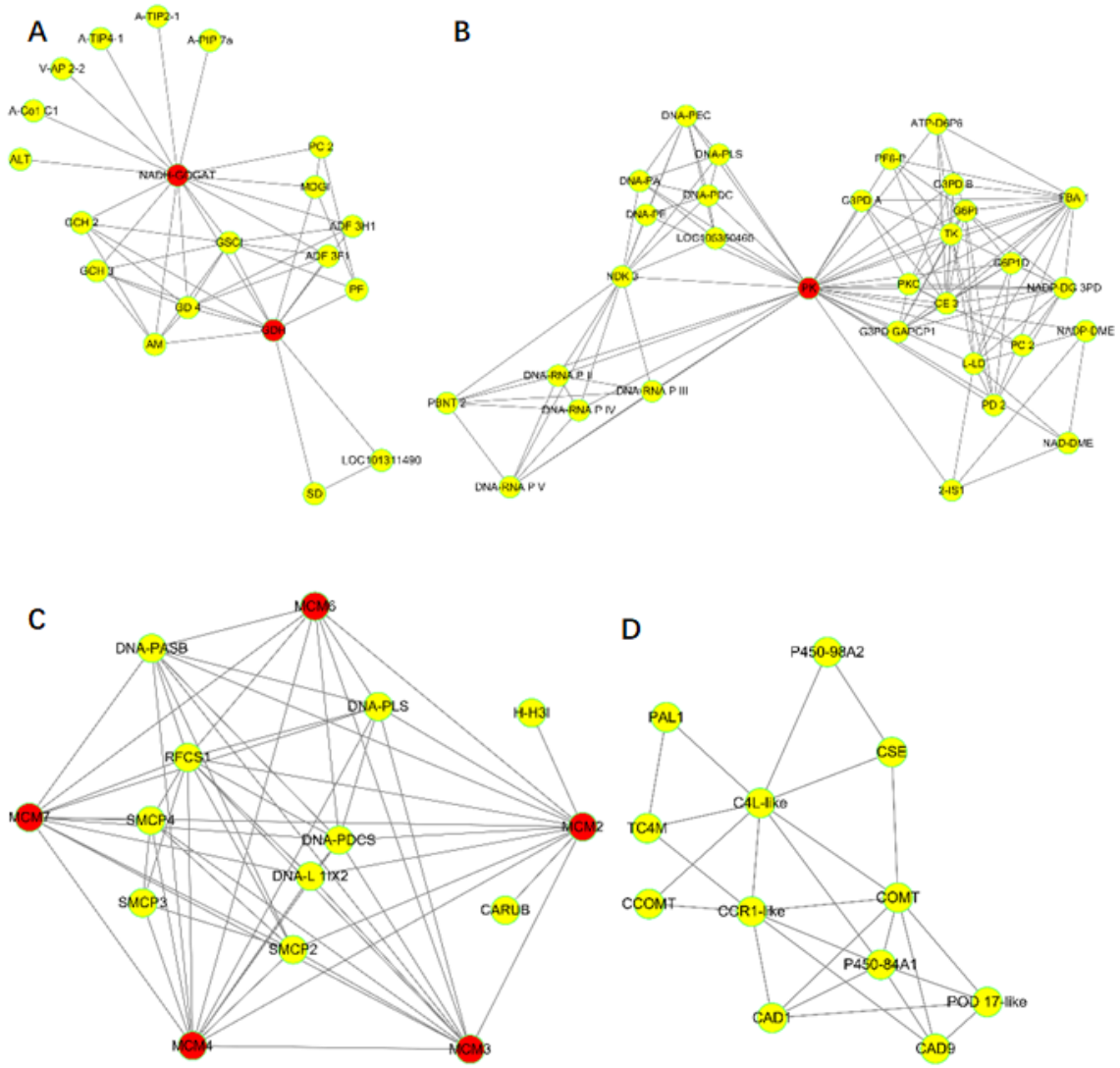

Figure 11

Protein-protein interaction (PPI) of the core proteins NADH-GOGAT, GDH (A) and PK (B), MCM 2-4 and 6-7 (C), as well as phenylpropanoid biosynthesis pathway (D). Abbreviations: A, vesicle-associated protein 2-2-like (V-AP 2-2), putative formamidase C869.04 isoform X1 (PF), probable aquaporin PIP-type 7a (A-PIP 7a), phosphoenolpyruvate carboxylase 2 (PC 2), malate dehydrogenase, glyoxysomal isoform X2 (MDGI), glycine cleavage system H protein 3, mitochondrial-like (GCH 3), glycine cleavage system H protein 2, mitochondrial (GCH 2), glutamine synthetase cytosolic isozyme (GSCI), glutamate synthase 1 [NADH], chloroplastic isoform X1 (NADH-GOGAT), glutamate dehydrogenase 1 (GDH), glutamate decarboxylase 4-like (GD 4), bifunctional 3-dehydroquinate dehydratase/shikimate dehydrogenase, chloroplastic-like (SD), aquaporin TIP4-1 (A-TIP4-1), aquaporin TIP2-1 (A-TIP2-1), aminomethyltransferase, mitochondrial (AM) , aldehyde dehydrogenase family 3 member H1-like (ADF 3H1), aldehyde dehydrogenase family 3 member F1 (ADF 3F1), acetyl-CoA carboxylase 1-like isoform X1 (A-Co1 C1), allantoinase (ALT); B, uncharacterized protein LOC105350465 (LOC105350465), transketolase, chloroplastic (TK), pyruvate kinase, cytosolic isozyme (PK), pyruvate decarboxylase 2 (PD 2), pyrophosphate-fructose 6-phosphate 1-phosphotransferase subunit alpha (PF6-P), probable DNA primase large subunit (DNA-PLS), polyribonucleotide nucleotidyltransferase 2, mitochondrial (PBNT 2), phosphoglycerate kinase, cytosolic-like (PKC), phosphoenolpyruvate carboxylase 2 (PC 2), nucleoside diphosphate kinase 3-like (NDK 3), NADP-dependent malic enzyme (NADP-DME), NADP-dependent glyceraldehyde-3-phosphate dehydrogenase (NADP-DG 3PD), NAD-dependent malic enzyme 59 kDa isoform, mitochondrial (NAD-DME), L-lactate dehydrogenase A (L-LD), glyceraldehyde-3-phosphate dehydrogenase GAPCP1 (G3PD

GAPCP1), glyceraldehyde-3-phosphate dehydrogenase B, chloroplastic (G3PD B), glyceraldehyde-3-phosphate dehydrogenase A, chloroplastic (G3PD A), glucose-6-phosphate isomerase 1, chloroplastic (G6PI), glucose-6-phosphate 1-dehydrogenase, cytoplasmic isoform 2 (G6P1D), fructose-bisphosphate aldolase 1, chloroplastic (FBA 1), DNA-directed RNA polymerases IV and V subunit 4 isoform X2 (DNA-RNA P IV), DNA-directed RNA polymerases II, IV and V subunit 11 (DNA-RNA P II), DNA-directed RNA polymerase V subunit 5A-like (DNA-RNA P V), DNA-directed RNA polymerase III subunit rpc4 isoform X1 (DNA-RNA P III), DNA polymerase epsilon subunit 3 (DNA-PE), DNA polymerase epsilon catalytic subunit A-like isoform X2 (DNA-PEC), DNA polymerase delta catalytic subunit (DNA-PDC), DNA polymerase alpha subunit B (DNA-PA), cytosolic enolase 3 (CE 3), ATP-dependent 6-phosphofructokinase 6 (ATP-D6P6), 2-isopropylmalate synthase 1, chloroplastic-like (2-IS1); C, DNA replication licensing factor MCM 2-4 and 6-7, probable DNA primase large subunit (DNA-PLS), structural maintenance of chromosomes protein 4-like (SMCP4), structural maintenance of chromosomes protein 2-1-like (SMCP2), replication factor C subunit 1 (RFCS1), structural maintenance of chromosomes protein 3 (SMCP3), histone H3.3 isoform X1 (H-H3I), hypothetical protein CARUB_v10021660mg (CARUB), DNA ligase 1-like isoform X2 (DNA-L 1IX2), DNA polymerase delta catalytic subunit (DNA-PDCS), DNA polymerase alpha subunit B (DNA-PASB); D, phenylalanine ammonia-lyase 1 (PAL1), caffeoylshikimate esterase (CSE), cytochrome P450 98A2 (P450-98A2), cinnamoyl-CoA reductase 1-like (CCR1-like), trans-cinnamate 4-monooxygenase (TC4M), 4-coumarate-CoA ligase 2-like (C4L-like), cytochrome P450 84A1 (P450-84A1), beta-glucosidase 44-like (BG-44-like), beta-glucosidase 42 (BG-42), probable cinnamyl alcohol dehydrogenase 9 (CAD9), peroxidase 17-like (POD 17-like), caffeic acid 3-O-methyltransferase (COMT), probable cinnamyl alcohol dehydrogenase 1 (CAD1), caffeoyl-CoA O-methyltransferase (CCOMT).

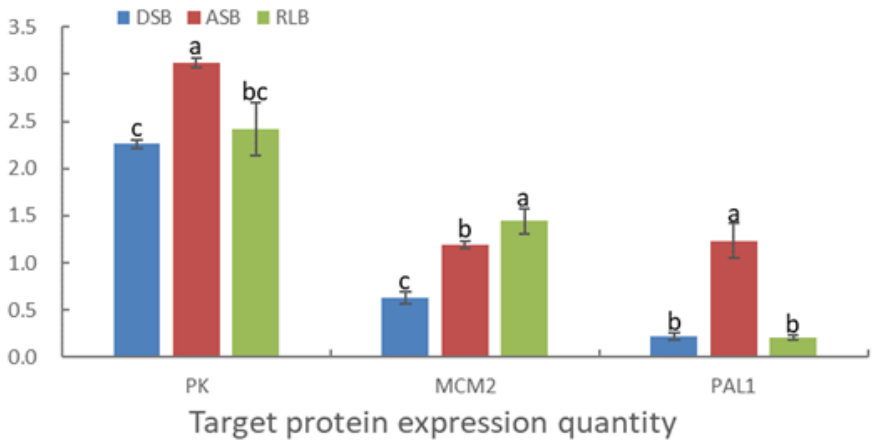

Figure 12

PRM verification of the expression quantities of target proteins PK, MCM2, and PAL1. DSB: dormancy shoot bud; ASB: activity shoot bud; RLB: ramet leaf bud; PK: pyruvate kinase; MCM2: minichromosome maintenance protein 2; PAL1: phenylalanine ammonia-lyase 1. Data are means and standard errors, of 3 groups of each type bud, and the experiment was repeated 3 times. Different letters in the same index means the significant difference among buds, separately ($P<0.05$). Bars represent the standard deviation (n=3).

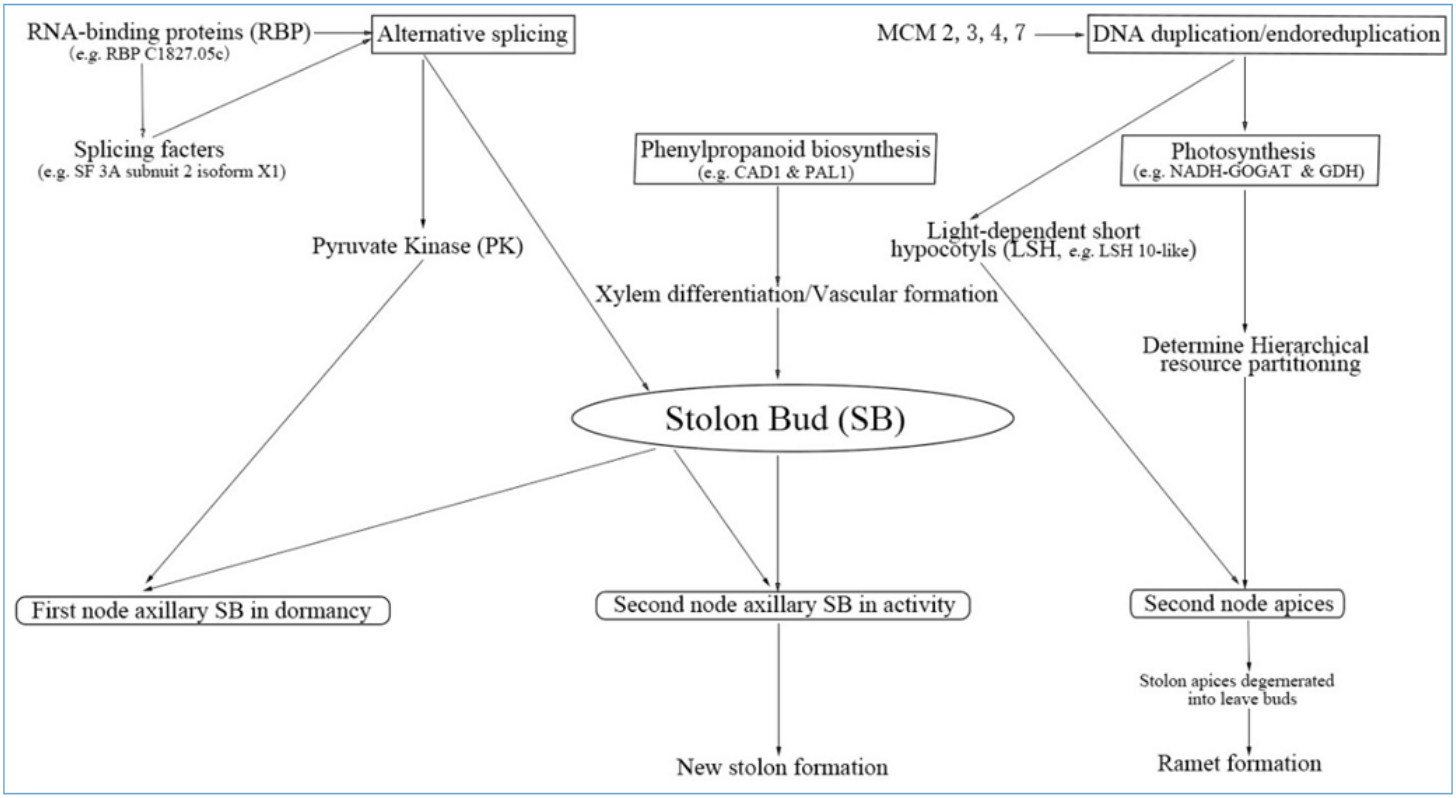

Figure 13

Possible mechanisms for differentially expressed proteins in regulating the heterogeneity of stolon buds in strawberry.

Supplementary Files

This is a list of supplementary files associated with this preprint. Click to download.

- supplement1.xls
- supplement2.xlsx
- supplement3.xlsx
- supplement3.xlsx
- supplement5.xlsx
- supplement6.xlsx
- supplement7.xlsx
- supplement8.xlsx
- supplement9.xlsx
- supplement10.xlsx
- supplement11.xlsx
- supplement12.xlsx
- supplement13.xlsx
- supplement14.xlsx
- supplement15.xlsx
- supplement16.docx

- supplement17.xlsx